REPORT DOCUMENTATION PAGE

Form Approved
OMB No. 0704-0188

1. AGENCY USE ONLY (Leave blank)	2. REPORT DATE	3. REPORT TYPE AND DATES COVERED
	June 1994	Final Report

4. TITLE AND SUBTITLE
Metallurgical Examination of Failed T-158 Cast Austempered Ductile Iron (CADI) Track Shoes

5. FUNDING NUMBERS

6. AUTHOR(S)
V. Champagne, M. Pepi, B. Pothier, D. J. Snoha, G. Wechsler, and M. G. H. Wells

7. PERFORMING ORGANIZATION NAME(S) AND ADDRESS(ES)
U.S. Army Research Laboratory
Watertown, MA 02172-0001
ATTN: AMSRL-MA-CB

8. PERFORMING ORGANIZATION REPORT NUMBER
ARL-TR-451

9. SPONSORING/MONITORING AGENCY NAME(S) AND ADDRESS(ES)
U.S. Army Tank-Automotive Command (TACOM)
Warren, MI 48397-5000

10. SPONSORING/MONITORING AGENCY REPORT NUMBER

11. SUPPLEMENTARY NOTES

12a. DISTRIBUTION/AVAILABILITY STATEMENT
Approved for public release; distribution unlimited.

12b. DISTRIBUTION CODE

13. ABSTRACT (Maximum 200 words)

The U.S. Army Research Laboratory (ARL), Materials Directorate (MD) conducted a metallurgical examination of prototype cast austempered ductile iron (CADI) tank track shoe bodies at the request of the U.S. Army Tank-Automotive Command (TACOM). The T-158 track bodies had failed during field testing on an M1/A1 battle tank. Each of the failed parts had been previously fitted with an ice cleat in service which most likely caused an undue stress concentration. The test results indicated that the failure was the result of poor part design and process control. The CADI track shoes had been fabricated according to the dimensional requirements of a forged component, instead of a separate cast design. The CADI material exhibited a variation in mechanical properties. Retained austenite measurements by X-ray diffraction correlated with the differences observed in mechanical properties. Chemical analysis revealed a high level of silicon which adversely affected the fracture toughness of the material. The CADI contained a low (but acceptable) nodule count and some of the nodules were flaked which decreased fatigue and impact resistance. Recommendations were made by ARL to redesign the track shoe utilizing casting technology criteria and to control the chemistry and microstructure.

14. SUBJECT TERMS	15. NUMBER OF PAGES
Metallurgical examination, Cast austempered ductile iron, Retained austenite	48
	16. PRICE CODE

17. SECURITY CLASSIFICATION OF REPORT	18. SECURITY CLASSIFICATION OF THIS PAGE	19. SECURITY CLASSIFICATION OF ABSTRACT	20. LIMITATION OF ABSTRACT
Unclassified	Unclassified	Unclassified	UL

BLANK PAGES
IN THIS
DOCUMENT
WERE NOT
FILMED

Contents

Figures

Tables

Background

The U.S. Army Tank-Automotive Command (TACOM) has investigated the possible use of cast austempered ductile iron (CADI) track shoe bodies for the M1 Abrams and Bradley Tanks. An FY90 TACOM program (CADI Tank Track) called for the development of CADI T-158 track shoes for use on the M1 Abrams tank. The objective of the track shoe program was to reduce the weight and/or cost of track shoes by replacing the forged parts currently used in the field, with those fabricated from CADI. A competitive contract for the production of T-158 track shoe assemblies with CADI shoe bodies was awarded to a contractor on September 26, 1990.

An entire strand of the T-158 track with the CADI shoe bodies was delivered to Ft. Greely, Alaska for field testing at the U.S. Army Cold Regions Test Center. Testing consisted of operating a 63-ton M1/A1 battle tank through mobile operations over a variety of terrain during the winter period of 1991-1992 [1]. One side of the vehicle had the CADI track while the normal fielded track (with steel shoes) was mounted on the other side. Temperatures during the test period ranged from +47°F to -52°F. Daily inspections of the track were performed during mobility testing, and failed CADI track shoe assemblies were replaced as needed. Five CADI track shoes failed during the mobility test and were replaced. Visible cracking of the shoe body was used as the failure criteria. Two additional CADI shoe bodies were found to be cracked during the final inspection after mobility testing. The accumulated mileage of each failed track component was recorded.

Along with the CADI T-158 shoe bodies, several other prototype components were installed on the vehicle during the cold regions field test. A modified ice cleat design was attached to every sixth track shoe in each strand during the mobility testing. It is important to note that ice cleats had been attached to every CADI T-158 track shoe body which failed at Ft. Greely. None of the shoe bodies without an ice cleat attached failed. After cold regions testing, the CADI T-158 track was shipped to Yuma Proving Ground (YPG) for additional mobility testing. Four of the CADI T-158 shoe bodies failed during these mobility tests at YPG. Whether these failed track shoes were previously fitted with ice cleats while at Ft. Greely was unrecorded. These four failures were not examined in this investigation.

After several months, two of the seven failed CADI track shoe bodies (Ft. Greely) were sent to the U.S. Army Research Laboratory-Materials Directorate (USARL-MD), Watertown, Massachusetts, for post-service analysis. Figures 1 and 2 show both of these track shoes in the as-received condition. Figure 1 shows Track #L30 (Ft. Greely designation stamped into shoe), while Figure 2 shows Track #R6 (also Ft. Greely designation). Track #L30 travelled 59 kilometers before failure, while Track #R6 travelled 1239 kilometers before failure.

Pertinent Specifications

The forged steel M1 track shoe is currently fabricated per U.S. Army Tank-Automotive Command (TACOM) Engineering Drawing No. 12348383. This drawing requires the material to be steel, forging alloy AISI 8640 or AISI 8740 Grade D, according to

MIL-S-46172. The forged steel is subsequently austenitized, quenched and tempered to a hardness of 30-37 HRC. However, the track shoes under investigation were fabricated from CADI to the requirements of ASTM A 897[2] Grade 150/100/7. The dimensions utilized in the fabrication of the track shoes by the contractor are shown in Figure 3. These dimensions were listed in a contractor report which was generated as part of their investigation of CADI as a track shoe alternative material. A contractor representative verified these dimensions, and also indicated that the CADI track shoes were fabricated in accordance with the forged steel drawing (TACOM Engineering Drawing 12348383). Initially, CADI Grade 175/125/4 (also known as Grade 3) was selected, however, this was revised by the contractor in an effort to improve toughness, while maintaining yield and tensile properties competitive with forged steel. The cast ductile iron track shoes were subsequently austenitized at 1650•F for 1-1/4 hr. and austempered at 625•F for 1-3/4 hr., for a target hardness range of 341-444 BHN (Grade 3). Specification ASTM A 897 states that this hardness range is not mandatory, and is listed for information only.

Dimensional Verification

The dimensions of the track shoe were inspected near the fracture origin region of each failed component. Track shoe #L30 failed at the bolt hole on the ground side (the only track shoe out of several failures to exhibit this type of fracture), while track shoe #R6 cracked along the "binocular tubes" on the ground side (the most prominent mode of fracture). Figure 4 shows schematically the regions where the dimensions were inspected for each of the failed track shoes. The dimensions for these areas were taken from the report generated by the contractor, which contained the drawings from which the track shoes were fabricated. The minimum allowable thickness of material adjacent to the bolt hole (crack initiation location of Track #L30) on the ground side is 0.33 +0.04/-0.02 inch (tolerance taken from U.S. Army Tank-Automotive Command (TACOM) Engineering Drawing No. 12348383, and also from the contractor report). This thickness narrows to 0.20 +0.04/-0.02 inch in some areas on the ground side. Track shoe #L30 met the minimum thickness requirements in this region.

The minimum allowable thickness of material in the center boss region of the "binocular tube" (crack initiation location of Track #R6) according to the contractor representative is:

$$\frac{[2.27" - (1.906" + 0.015")]}{2} = 0.1745"$$

Again, this is the same minimum allowable thickness noted on TACOM Engineering Drawing No. 12348383 for a *forged* component. Since the thickness varied around the diameter of the tube, macrographs were taken of a representative cross section showing the area of minimum thickness and the ground side thickness for Track #R6. Figure 5 shows the area of minimum thickness of track shoe #R6, while Figure 6 shows the thickness at the ground side. The thickness of these regions was measured directly from the photomicrographs, at a magnification of 10x. The thickness results are listed in Table 1, as well as the minimum allowable criteria from TACOM drawing No. 12348383.

Table 1
Track Shoe Thickness Results

Track Shoe	Region	Thickness (inch)	Minimum Allowable Thickness (inch)
#R6	ground side	0.153	0.1745
#R6	minimum	0.138	0.1745

The thickness measured (the ground side and minimum thickness) at the "binocular tube" region of track shoe #R6 was below the minimum requirement specified on the *forged component* drawing by as much as 20%.

Visual Examination and Light Optical Microscopy - Track Shoe #L30

Figure 7 shows the failed half of the track shoe. The location of the crack was on the ground side. The track shoe was sectioned in order to examine the fracture surfaces, as shown schematically in Figure 8. These fracture surfaces were labelled A, B, C and D for identification purposes. Each fracture surface was covered with a vast amount of corrosion products, indicating a prolonged exposure to the environment. Figure 9 shows fracture faces A and B respectively. Fracture face C is shown in Figure 10, while fracture face D is shown in Figure 11. Although the fracture faces were covered with corrosion, fractographic features were still discernable. The chevron patterns and river markings of each fracture surface indicated the fracture initiated at the bolt hole (ground side). Figure 12 shows a magnified view of the crack through the bolt hole region (ground side). This hole is utilized to attach the ice cleat to the track shoe. Figure 13 shows a magnified view of the underside of the cracked bolt hole region (wheel side). This hole was examined, in order to reveal anomalies which may have contributed to crack initiation. It was noted that the top 1/16 inch of this hole contained what appeared to be a start of a thread (Figure 12). The TACOM drawing for a forged component does not require this bolt hole to contain threads or a chamfer, as it is solely a through-hole. Figure 14 shows the comparison between the bolt hole of track shoe #R6 and that of track shoe #L30. The bolt hole of track shoe #R6 contained no such markings. In addition, significant wear was noted on the underside of the hole, most likely the result of a washer or bolt head. Magnetic particle inspection was performed on this hole to reveal possible evidence of cracking. Figure 15 is a blacklight photograph showing the wear, as well as a crack (as denoted by the arrow) . Figure 16 is a photomicrograph of the fracture origin, as noted on Fracture Face B. Figure 17 shows an enlargement of the crack origin, as noted on Fracture Face D.

Visual Examination and Light Optical Microscopy - Track Shoe #R6

Figure 18 shows the failed half of the track shoe. The crack initiation site occurred on the ground side of each binocular tube. Figure 19 shows an end view of the cracking. Figure 20 schematically illustrates the method of sectioning for the second failed track shoe. The fracture faces were labelled A, B, C and D. Segment A1 broke into two pieces upon sectioning, and was labelled as A1a and A1b. As with track shoe #L30, the fracture surfaces were heavily corroded, but some fractographic features were still discernible. Figure 21 is a montage showing fracture face A and fracture face C. The chevron pattern and river markings indicated the fracture initiated in the region designated by the arrow. This region was on the ground side of the track shoe. Similarly, Figure 22 is a montage of fracture face B and D. Again, the chevron pattern and river markings revealed the fracture origin to be the location designated by the arrow. Figures 23 and 24 are magnified views of the fracture origins (from fracture face A and B , respectively). No obvious surface anomalies were noted at either of the fracture origin sites.

Scanning Electron Microscopy

The fracture surfaces of each of the failed track shoes were examined utilizing the scanning electron microscope. Figure 25 shows the difficulty encountered, due to the corroded surfaces. This photomicrograph shows the "mud cracking" feature of the surface. The fracture surface was chemically cleaned, revealing a more discernible morphology. Figure 26 shows the fracture morphology of a less corroded region. Note the craters where the graphite spheroids have been pulled out. The surface appears to have failed in cleavage. Areas of ductile dimples were noted, and are shown in Figures 27 and 28. These dimples are associated with a ductile failure which could occur during overload.

For comparative purposes, the fracture surfaces of laboratory tested tensile and impact specimens were examined utilizing the SEM. Both the tensile and impact fracture surfaces were similar. Figure 29 shows the fracture surface of an impact specimen at low magnification. Note the graphite spheroids, and the pits left by the pulled-out spheroids. Figure 30 shows this region at higher magnification. Note the ductile dimples surrounding the graphite spheroids.

Chemical Analysis

The track shoes were specified to be fabricated from cast austempered ductile iron conforming to the requirements established in ASTM A 897. Although this specification does not list specific chemical requirements, it is stated that *such requirements may be agreed upon between the manufacturer and the purchaser.* The chemical compositional requirements established by the manufacturers are listed in Table 2, as well as the chemistry of each component. Atomic absorption and inductively coupled argon plasma emission spectroscopy were utilized to determine the chemical composition of the alloy. The carbon and sulfur content was analyzed by the Leco combustion method. Samples representing a "thick" and "thin" section of the castings were analyzed from each of the two failed track shoes. In general, the composition of the material under investigation compared favorably with the acceptable criteria, although the

silicon content of each track shoe was slightly higher than specified. Also noted, was the fact that chromium, molybdenum, titanium and copper were all higher than the residual criteria for each track shoe. High levels of these elements may be attributed to the scrap iron used in the ADI melt. The material from Track #30 Thin, had an abnormally high chromium level, which was very much in excess of the residual acceptance criteria. Although having minimal affect on mechanical properties, this excess in particular elements suggests a poor chemical control on behalf of the manufacturer.

Table 2 Chemical Compositions
Weight Percent

Element	Track #L30 Thin	Track #L30 Thick	Track #R6 Thin	Track #R6 Thick	Acceptance Criteria
Carbon	3.70	3.72	3.63	3.64	3.2-3.8 AIM 3.6
Silicon	2.70	2.83	3.04	2.98	2.45-2.65 AIM 2.50
Manganese	0.090	0.084	0.089	0.094	0.30 max.
Phosphorus	0.024	0.014	0.016	0.020	0.03 max.
Sulfur	0.002	0.006	0.005	0.006	0.015 max.
Nickel	1.31	1.37	1.49	1.47	1.2-1.5
Chromium	0.12	0.057	0.052	0.061	residual
Molybdenum	0.004	0.002	0.002	0.002	residual
Titanium	0.030	0.026	0.026	0.030	residual
Copper	0.029	0.031	0.023	0.021	residual
Magnesium	0.050	0.040	0.040	0.050	AIM 0.035
Iron	remainder	remainder	remainder	remainder	remainder

Metallographic Examination

Regions representing "thin" and "thick" areas of the casting were sectioned from each of the failed track shoes and prepared for metallographic examination, as shown schematically in Figure 31. This diagram shows a total of eleven samples which were sectioned from a portion of failed track shoe #L30 for metallographic samples and retained austenite measurement samples. Similar specimens were sectioned from track shoe #R6. Examination in the as-polished condition and at low magnification (12.5x) revealed a very large shrinkage cavity within a thick region from track shoe #L30, as shown in Figure 32. The graphite spheroids were shown to be evenly distributed within the matrix (Figure 33). The nodules differ in size significantly which suggests that some may have formed early in the casting process while other formed later by post inoculation. However, the difference in sizes could also be due to a "slicing effect", in which different portions of the randomly distributed nodules were sectioned. In addition, some flaked nodules were noted. In excess, these irregularly shaped nodules are undesirable, since the larger surface to volume ratio raises the notch sensitivity and lowers the fatigue and impact resistance of the casting. Figure 33 was used to classify the graphite size per ASTM A 247 [3], *Method for Evaluating the Microstructure of Graphite in Iron Castings*. The average graphite dimension measured was within the 5-6 size class. The average nodule count measured from three samples of each track shoe was approximately 132 per sq. mm. nodules, which is considered acceptable. although slightly less than optimal for Grade 150/100/7 CADI.

The microstructure of CADI following the austempering process for Grade 150/100/7 CADI per ASTM A 897 should consist of an even dispersion of graphite spheroids in a matrix of acicular ferrite and carbon-rich austenite, which has been termed ausferrite. A 4% Picral etchant was applied to the polished surfaces of the samples, in order to examine the resultant structure. The etched microstructure revealed the graphite spheroids in a matrix of what appeared to be ausferrite (Figure 34). It was difficult to discern the microstructure of the etched CADI through use of black and white photomicroscopy. The CADI industry utilizes color photomicroscopy when inspecting the structure of CADI. A widely accepted method of heat tinting [4] was utilized by ARL to colorize the microstructure. This method consists of mechanically polishing a section of CADI through silicon carbide papers of ascending grit count (180, 320, 400, 600). The samples were further polished on a pelon cloth utilizing a 0.5 micron alumina solution. The samples were subsequently etched with 2% Nital, and placed within a furnace at 500°F for four hours, until a blue-black tint was noted on the etched surface.

The heat tinting technique caused each phase associated with the material to oxidize to a different color. Referring to a representative micrograph at 100x (Figure 35), the blue region represents unreacted retained austenite, an undesirable phase. This phase is usually located within the "last-to-freeze (LTF)" region, and acts as the weak link upon exposure to cold temperatures or loading, since it is prone to transformation to martensite upon cooling or applied high stress. The white dots represent the graphite nodules. The reacted high carbon stabilized austenite tinted purple. Referring to the representative micrograph of the track shoe material at 1000x (Figure 36), the unreacted retained austenite tinted blue, the reacted, high carbon stabilized austenite tinted purple, the ferrite tinted white, the eutectic carbide tinted beige, and the martensite shows as dark blue needles.

Retained Austenite Measurement

X-Ray diffraction retained austenite measurements were performed on representative samples of both failed track shoes (#L30 and #R6) utilizing the Technology for Energy Corporation (TEC) Model 1610 X-Ray Stress Analysis System. Based on ASTM Standard E 975 [5], *X-Ray Determination of Retained Austenite in Steel with Near Random Crystallographic Orientation*, TEC's retained austenite analysis software compares the measured integrated intensity of the diffraction peaks from the martensite/ferrite alpha-phase and austenite gamma-phases with calculated theoretical intensities. Quantification of the martensite/ferrite and austenite volume fractions is possible because the total integrated intensity of the diffraction peaks for each phase is proportional to the volume fraction of that phase. Other crystalline phases, such as carbides, may generate diffraction peaks of sufficient intensity and at angular positions so as to interfere with the martensite/ferrite and/or austenite peaks resulting in a biased percent retained austenite measurement. For this reason, the volume fraction of carbide or other phases (and in this material, graphite nodules) should be determined. The TEC software requests the percent volume of carbides in the sample as part of the analysis setup.

Four specimens from each failed track shoe were sectioned utilizing a water-cooled diamond saw. These samples were denoted as #L30- and #R6- "A" through "D", and were taken from similar locations on the track shoes. Standard metallographic grinding and polishing methods were employed in preparing the Bakelite-mounted specimens for image and X-ray analysis. All retained austenite measurement data were obtained with the TEC Stress Analyzer in the parafocusing configuration, and from the diffraction of chromium K-alpha radiation from the (211) and (200) crystallographic planes of the alpha-phase martensite/ferrite and the (220) and (200) planes of the gamma-phase austenite. The specimens were irradiated at the surface with an approximate 4mm round spot size at two arbitrarily chosen locations and orientations. Four degrees of psi-oscillation was activated for each measurement to circumvent coarse grain effects that could be encountered in this cast material. The Buehler Omnimet II Image Analysis generated a graphite nodule percent area of 11.1% +/- 0.6% (average of four readings from two each #L30 and #R6 specimens). These results were incorporated in the TEC measurement program as carbide percentage. National Institute of Standards and Technology (NIST) 5, 15 and 30 percent austenite in ferrite standard reference materials 485a, 486 and 487, respectively, were used as a means of determining X-ray measurement accuracy and repeatability. Measurements were performed on these standards on three separate occasions.

Table 3 lists the X-ray diffraction retained austenite measurement results. An approximately uniform austenite volume fraction was determined in both track shoes regardless of where the specimens were sectioned from the track shoes or the X-ray measurement location or orientation. However, the #L30 retained austenite percentage is somewhat higher on average than the #R6 (27.4% compared to 24.3%). Graphite nodule content, shrinkage porosity just below the X-ray irradiated surface or sample preparation (temperature or deformation transforming the retained austenite to martensite) could account for this difference, but more likely, it can be attributed to a variation in the chemical composition and possibly the heat treat process from one track shoe to the other. No significant preferred crystallographic orientation, coarse grain size nor carbide interference in the diffraction pattern was detected during this X-Ray investigation. Referring to SAE Special Publication 453 [6], *Retained Austenite and Its Measurements By X-Ray Diffraction*, the ratio of the integrated intensities of the austenite gamma-phase (220) and (200) diffraction peaks should be between 1.2 and 1.8. If the ratio is outside this range by more than 200%, a severe preferred orientation or coarse grain size is present in the specimen. Almost half of all calculated alpha-phase integrated intensity ratios fell within the acceptable range, while the remaining ratios were out of range by far less than the 200% limit, averaging 39% +/- 17%. Additionally, the results of a martensitic/ferritic phase residual stress measurement made with a chromium K-alpha radiation and the sine-squared psi method utilizing ten positive psi-angles further indicated that neither of these severe texture effects existed. Though polishing-induced stress was measured, the supplemental relative integrated intensity data, (uniform and averaging 2,147 +/- 61 for all ten psi-angles) suggested a random or near random orientation. Smooth, consistent diffracted peak shapes, evidence of other than a coarse grain structure, were observed throughout the retained austenite and residual stress data collections. These results were anticipated since castings have little preferred orientation.

Table 3
Retained Austenite Measurement results from NIST
Standard Reference Materials and CADI #L30 and #R6 Specimens

Specimen	Measurement Location	Retained Austenite (%)
NIST 5% Standard 485a (ID 056, 4.40%)	Center	4.3 +/- 0.2
NIST 15% Standard 486 (ID 462, 14.72%)	Center	13.4 +/- 0.6
NIST 30% Standard 487 (ID 105, 31.32%)	Center	29.9 +/- 0.9
#L30A	1	27.0
	2	25.5
#L30B	1	26.6*
	2	28.3*
#L30C	1	28.5
	2	29.0
#L30D	1	26.9
#R6A	1	23.9
	2	24.2
#R6B	1	26.1
	2	26.4
#R6C	1	24.1
	2	22.7
#R6D	1	22.8
	2	23.8

* - Average of two measurements

Note: #L30D specimen size prohibited a second measurement location

The TEC method of carbide interference, preferred orientation and/or coarse grain size evaluation included the alpha-phase martensite/ferrite (211) and (200) diffraction peaks integrated intensity ratio along with the austenite intensity ratio as stated above (except for TEC's acceptance range of 1.1 - 1.8). The martensite/ferrite ratio for these two peaks should be between 8 and 11. All of the track shoe specimens alpha-phase integrated intensity ratios were below this range with the values falling between 6.2 and 7.8 for an out of range average of 15% +/- 6%. This suggests that the alpha-phase (200) peak contained carbide reflections. However, if the 200% out of range limit is appropriate for the martensite/ferrite intensity ratio as with the austenite ratio, then the interference from the carbides could be considered negligible. (It should be noted that the TEC, ASTM standard and SAE publication retained austenite measurement procedures, integrated intensity ratio acceptance ranges and theoretical relative intensity factors were developed or calculated for steels. Therefore, the results and analyses reported herein should be objectively viewed and are presented as a cursory X-Ray investigation of retained austenite in austempered ductile iron).

Mechanical Properties

Mechanical testing was performed on specimens sectioned from each of the failed track shoes. ASTM A 897 specifies tensile property requirements including ultimate tensile strength, 0.2% yield strength and percent elongation. These properties apply only after the austempering heat treatment. The same region of track shoe was used in the fabrication of specimens from both track shoe #L30 and #R6, as shown schematically in Figures 37 and 38, respectively. In addition, hardness testing, fracture toughness testing and Charpy impact testing were performed. In each case, the largest possible specimens were fabricated. However, due to geometrical restrictions, the tensile, fracture toughness and impact specimens were subsized.

Tensile Testing

Tensile coupons were sectioned as shown in Figure 39, and tested in accordance with ASTM E 8[7], *Test Method of Tension Testing of Metallic Materials (Subsize)*. The results of tensile testing are listed in Table 4. Specimens were tested on a 20,000-lb capacity Instron universal electromechanical test machine, with a 5,000-lb load cell. A crosshead speed of 0.05 inches/minute was utilized, and a 1/2 inch-10% extensometer was used to measure strain.

Table 4
Tensile Test Results
Tensile Coupons from Track Shoes #L30 and #R6
20,000-lb Instron Electromechanical Machine
Room temperature

Specimen ID	0.2% Yield (psi)	UTS (psi)	%RA	%EL
#L30A	122,120	140,030	2.0	6.3
#L30B	114,870	137,200	2.6	4.0
#L30C	124,120	160,270	9.0	12.3
#L30D	122,400	159,830	8.6	9.2
#R6A	136,050	179,940	5.4	7.0
#R6B	138,280	184,790	6.3	8.6
#R6C	143,780	185,040	6.8	7.4
#R6D	141,150	184,130	7.2	9.8
Acceptance (Grade 2)	100,000	150,000	N/A	7.0
Acceptance (Grade 3)	125,000	175,000	N/A	4.0

Specimens #L30A and #L30B failed to meet the specified UTS and elongation requirements for Grade 2. Specimens #L30C and #L30D conformed to the governing specification for Grade 2 with respect to each of the requirements. Each specimen sectioned from track shoe #R6 conformed to the governing specification for Grade 3. In general, the results suggested that specimens fabricated from the second failed track shoe were higher in strength than those fabricated from the first failed track shoe. Results from track shoe #R6 specimens agreed with

those of CADI specimens tested by the contractor, in yield strength and UTS. However, the %EL of the #R6 specimens were slightly lower than the contractor results. Note the variability between the specimens sectioned adjacent to each other from track shoe #L30.

Hardness Testing

Although hardness requirements were not specified for this material, hardness testing was performed for informational purposes. Table 5 lists the results of hardness tests performed within the tab region of each of the four tensile coupons from track shoes #L30 and #R6, respectively.

Table 5
Rockwell "C" Macrohardness Test Results
Tensile Coupons from Track Shoes #L30 and #R6
Room Temperature
150 kgf load
Diamond Penetrator

Sample ID	HRC	Sample ID	HRC
#L30A	32.4	#R6A	37.1
	32.5		37.2
	31.8		37.6
	32.2		37.0
#L30B	32.5	#R6B	37.7
	32.3		37.7
	31.9		38.0
	32.2		37.9
#L30C	32.6	#R6C	37.9
	32.3		37.5
	32.3		37.4
	32.1		36.0
#L30D	31.9	#R6D	36.0
	31.6		37.0
	32.2		37.7
	32.9		37.5
Average	32.2		37.3
ASTM A 897*:	37-47 HRC	ASTM A 897*:	37-47 HRC

* - This hardness value for Grade 150/100/7 CADI is not mandatory.

The hardness values from #R6 specimens were greater than those of #L30 specimens by over five Rockwell "C" points. At this range of hardness, that translates to an approximate 20,000 psi increase in UTS (from standard hardness conversion charts). This value is consistent with the magnitude of increased strength noted from #R6 specimens as compared to the strength of #L30 specimens. It should also be noted that the values of hardness from #R6 specimens just meet the ASTM typical hardness range of 37-47 HRC (converted from Brinell 341-444), in contrast with the results from #L30 specimens, which fell below this guideline.

Fracture Toughness Testing

Fracture toughness coupons were sectioned as shown in Figure 39 and tested per ASTM E 813 [8], *Test Method for J_{IC}, a Measure of Fracture Toughness*. The three-point bend specimens were precracked at 30 Hz. using a 20,000-pound capacity Instron servohydraulic test machine. The crack sizes were measured on each side of the specimen and were as follows:

Sample	Crack Sizes (in.) Side A	Side B	Cycles
#L30A	0.0518	0.0386	1700
#L30B	0.0500	0.0322	2100
#R6A	0.0517	0.0513	2600
#R6B	0.0546	0.0443	1500

The specimens were subsequently tested on the 20,000-pound capacity Instron electromechanical test machine at 0.02 inch/minute crosshead speed. A 0.100 inch opening crack gage was utilized to obtain the load-crack opening displacement plot. ASTM E 399 [9], *Test Method for Plane-Strain Fracture Toughness of Metallic Materials was* referenced in analyzing the data. The following results were obtained:

Sample	P_Q	P_{MAX}	P_{MAX}/P_Q
#L30A	192	249	1.26
#L30B	183	263	1.44
#R6A	200	253	1.29
#R6B	181	233	1.30

One criterion states that P_{MAX}/P_Q must be less than 1.10. These specimens did not meet this criterion, thus these data are invalid, according to ASTM E 399. The values of K_Q were found to be as follows:

Sample	K_Q (ksi$\sqrt{in.}$)	x 2
#L30A	35.5	71.0
#L30B	36.0	72.0
#R6A	43.3	86.6
#R6B	42.1	84.2

The K_Q was doubled since subsize specimens (1/2 the size of standard specimens) were tested. These results are consistent with those obtained on specimens tested at Benet Laboratories [10] in a similar effort. The Benet Laboratories results ranged from 76 to 82 ksi$\sqrt{in}$.

Charpy (Simple-Beam) Impact Testing

Figure 40 shows the notched and unnotched specimens which were sectioned from the failed track shoes and tested in accordance with ASTM E 23 [11], *Test Methods for Notched Bar Impact Testing of Metallic Materials*. Each specimen was tested on the 240 ft-lb capacity Satec impact machine. Lifts were utilized to maintain proper specimen height within the machine. The results of this testing are listed in Table 6.

Table 6
Charpy Impact Testing Results
Impact Coupons from Track shoes #L30 and #R6
240 ft-lb Satec Impact Machine
Room Temperature
Half-Sized Specimen (t = 0.197 inch)

Sample ID	Condition	Impact Energy (ft-lbs)	x 2 (ft-lbs)
#L30A	notched	4.0	8.0
#L30B	notched	4.0	8.0
#L30C	unnotched	40.0	80.0
#L30D	unnotched	41.0	82.0
#R6A	notched	2.7	5.4
#R6B	notched	2.5	5.0
#R6C	unnotched	35.0	70.0
#R6D	unnotched	19.0	38.0
ASTM A 897-90 Grade 150/100/7	unnotched		60.0

The impact energy was doubled since subsize specimens (one-half the size of standard specimens) were tested. The unnotched specimens tested met the requirement set forth in ASTM A 897 for Grade 150/100/7 Charpy bars tested at 70• +/- 7•F, with the exception of Sample #R6D. The results from track shoe #L30 specimens are higher in magnitude than the results from track shoe #R6 specimens. This correlates to the hardness and tensile results, since, in general, a material with lower strength and elongation (more ductile) will have a higher impact resistance than a stronger (more brittle) material.

Discussion

The CADI track shoes had been fabricated according to the dimensional requirements of the forged component. In fact, the same engineering drawing was used. The yield and ultimate tensile strengths of the specified steel forging alloy AISI 8640 or 8740, Grade D, are comparable to those of CADI, Grade 175/125/4. However, the percent elongation and percent reduction in area differ substantially. The forged AISI 8640 or 8740 alloy can expect to display a percent elongation close to 20%, and a percent reduction in area of approximately

50%. This is much greater than the CADI value of 4-7% elongation (Grades 175/125/4 and 150/100/7, respectively). This significant lack of ductility would adversely affect the impact resistance of the CADI in service. Taking this into consideration, it would seem appropriate that a separate design would have to be developed for the CADI material. Otherwise, how else can a fair assessment be made of CADI?

The new design would need to take into account the appropriate casting gates and risers. The cross sectional thickness of the new CADI design would most likely have to be increased at particular areas of higher stress. Evidence substantiating this claim is shown by the cracking of track shoe #R6 which initiated at the ground side of the binocular tube section. This region did not even conform to the engineering drawing of the forged component as required and was found to be dimensionally under tolerance by approximately 0.022 inch. The CADI track shoes that were analyzed contained several regions where a thick section abruptly transitioned into a thin one and would have different rates of cooling during casting. This condition caused internal shrinkage cavities to form which were noted on the CADI components during metallographic examination. These cavities were relatively large, encompassing areas approximately 1/4" x 3/4". Overall, the track shoe design (although proven for a forged component) may not be favorable with respect to a casting.

Each of the failed track shoes was fitted with an ice cleat in service suggesting that an undue stress concentration may have existed. Cracking was not confined to a specific region (the track shoe #L30 failure initiated at the bolt hole on the ground side, while track shoe #R6 cracked across the two "binocular tubes") which may indicate a design problem. The deep grooves found on the edge of the bolt hole of track shoe #L30 may have been threads machined by mistake, marks left by impact from the cleat bolt (allowed to rub against this area), wear caused by service life, or simply a poor chamfer. In any case, the marks may have created an undue stress concentration thus initiating failure.

Fractographic analysis revealed that the crack origin was located at the bolt hole (ground side) on track shoe #L30. The crack initiation site was found to be on the ground side of each binocular tube on track shoe #R6. Ductile dimples were observed on areas of the fracture surface which were only reconciled after chemically removing some of the heavy corrosion product.

Chemical analysis revealed a high level of silicon in each of the samples investigated. This could have been due to an addition of ferrosilicon, utilized to boost the nodule count during production. A higher than nominal silicon content is less than optimal, since the fracture toughness properties of CADI decrease with the increase of silicon. In addition, chromium, molybdenum, titanium and copper were all higher than the specified limits. Although the deleterious affects of higher levels of these elements are minimal, it does suggest poor manufacturer chemical control.

Metallographic examination of representative samples of the failed track shoes revealed a somewhat low nodule count for Grade 150/100/7 CADI. This deficiency also tends to affect the mechanical properties of this material. In addition, some of the nodules were "flaked",

which is not an optimal shape. This shape consists of a high surface to volume ratio, which tends to increase the notch sensitivity of the material, while decreasing the fatigue and impact resistance. The etched and heat tinted structure of the CADI samples resembled the typical structure of CADI.

Retained austenite measurements were performed, revealing contents of 27.4% for track shoe #L30 and 24.3% for track shoe #R6. This difference in retained austenite content correlated to the difference in strength noted between the two shoes.

A variation in mechanical properties between both the #L30 and #R6 samples was noted. The tensile properties of #L30 specimens were slightly lower than those of #R6. The UTS of two #L30 specimens fell below the acceptable criteria, as did the %EL of two #L30 specimens. The values attained for the #L30 specimens had a relatively large spread, for a supposed homogeneous material. Each #R6 tensile specimen obtained values conforming to the acceptable criteria of ASTM A 897. Macrohardness testing (although not mandatory according to ASTM A 897) showed that track shoe #R6 specimens met the minimum requirement, while track shoe #L30 specimens fell well below the lower limit. Fracture toughness testing showed #R6 could withstand fracture better than #L30 specimens. Both track shoes conformed to the allowable impact energy for unnotched specimens.

Conclusion

The test results of the metallurgical investigation conducted on two cast austempered ductile iron T-158 M1 tank track shoes that were field tested at Fort Greely, Alaska, suggested that the failure was the result of poor part design and process control. The ADI material from the two shoes exhibited a considerable variation in mechanical properties. These differences were most likely caused by variations in the structure and composition of the castings before the austempering heat treatment. A higher than optimal silicon content decreased the impact resistance of the track shoes. Moreover, the CADI track shoes were fabricated according to the forged steel engineering drawing. A separate CADI drawing should be developed incorporating a thicker cross section to increase impact resistance. Some section thicknesses in the region of cracks were considerably below the requirements of the forged component drawing. The combined lower ductility and impact resistance of CADI compared to the forged steel and the reduced section thickness reduced the load bearing capacity of the CADI track shoes.

Recommendations

It was not the purpose of this failure investigation to dismiss CADI as a viable track shoe material. Too many external factors unrelated to CADI led to these failures, making it difficult to blame them on the material itself, such as:

*The additional stress induced by the attached ice cleats,

*The overall design of the track shoe with respect to casting,

*The CADI shoe fabricated to the same dimensions as the forged shoe,

*The dimensional undertolerance of the CADI shoe in some areas,

*Poor manufacturing techniques (i.e., additional silicon, some flaked nodules) led to sub-par mechanical properties for track shoe #L30.

A fairer assessment of the use of CADI in this application would occur if each of the above factors were addressed.

Acknowledgements

The authors wish to thank George Dewing and Jack Mullin for sectioning and metallography, respectively, Raymond Hinxman and Kyu Cho for X-Ray Diffraction, Robert Pasternak and Karen Harvey for mechanical testing, and John Keough for valuable processing information. With the exception of John Keough, who represents Applied Process Inc., each are employed by the U.S. Army Research Laboratory, Watertown, Massachusetts.

References

1. Muth, B.W., *Abbreviated Test Report for the Preproduction Qualification Test (PPQT) of Product Improvements for the M1A1 Tank System*, U.S. Cold Regions Test Center, Unit 45818, APO AP 96508-7850, USATECOM Project No. 1-VC-080-1A1-152, May 1992.

2. *Specification for Austempered Ductile Iron Castings*, ASTM A 897, Volume 01.02, Ferrous Castings; Ferroalloys.

3. *Method for Evaluating the Microstructure of Graphite in Iron Castings*, ASTM A 247, Volume 01.02, Ferrous Castings; Ferroalloys.

4. Kovacs, B.V., Sr., *Heat Tinting of ADI Microstructures*, Atmosphere Furnace Company-Technical Center, Livonia, Mississippi.

5. *X-ray Determination of Retained Austenite in Steel with Near Random Crystallographic Orientation*, ASTM E 975, Volume 03.01, Metals-Mechanical Testing; Elevated and Low-Temperature Tests; Metallography.

6. SAE Special Publication 453, *Retained Austenite and its Measurements by X-ray Diffraction*,

7. *Test Methods of Tension Testing of Metallic Materials*, ASTM E 8, Volume 03.01, Metals-Mechanical Testing; Elevated and Low-Temperature Tests; Metallography.

8. *Test Method for J_{IC}, a Measure of Fracture Toughness*, ASTM E 813, Volume 03.01, Metals-Mechanical Testing; Elevated and Low-Temperature Tests; Metallography.

9. *Test Method for Plane-Strain Fracture Toughness of Metallic Materials*, ASTM E 399, Volume 03.01, Metals-Mechanical Testing; Elevated and Low-Temperature Tests; Metallography.

10. Fracture Toughness Indicators for ADI, Benet Laboratories.

11. *Test Methods for Notched Bar Impact Testing of Metallic Materials*, ASTM E 23, Volume 03.01, Metals-Mechanical Testing; Elevated and Low-Temperature Tests; Metallography.

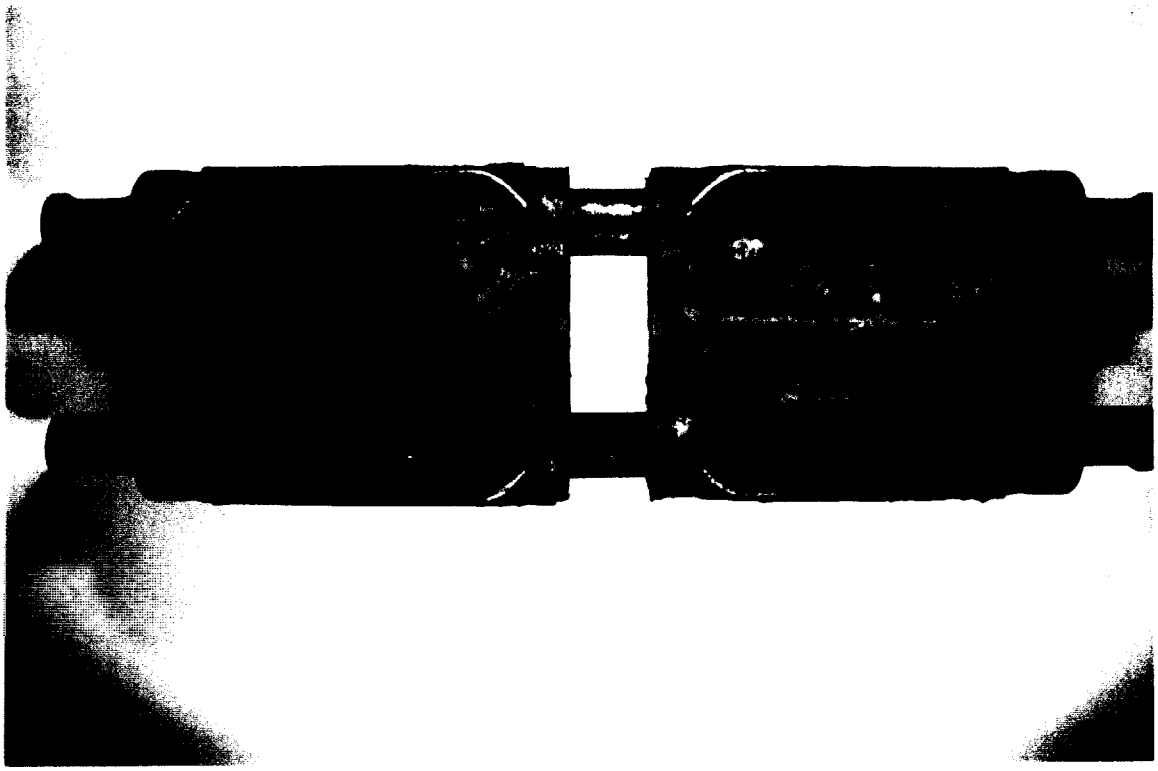

FIGURE 1 Failed track shoe #L30 in the as received condition. Reduced 80 %

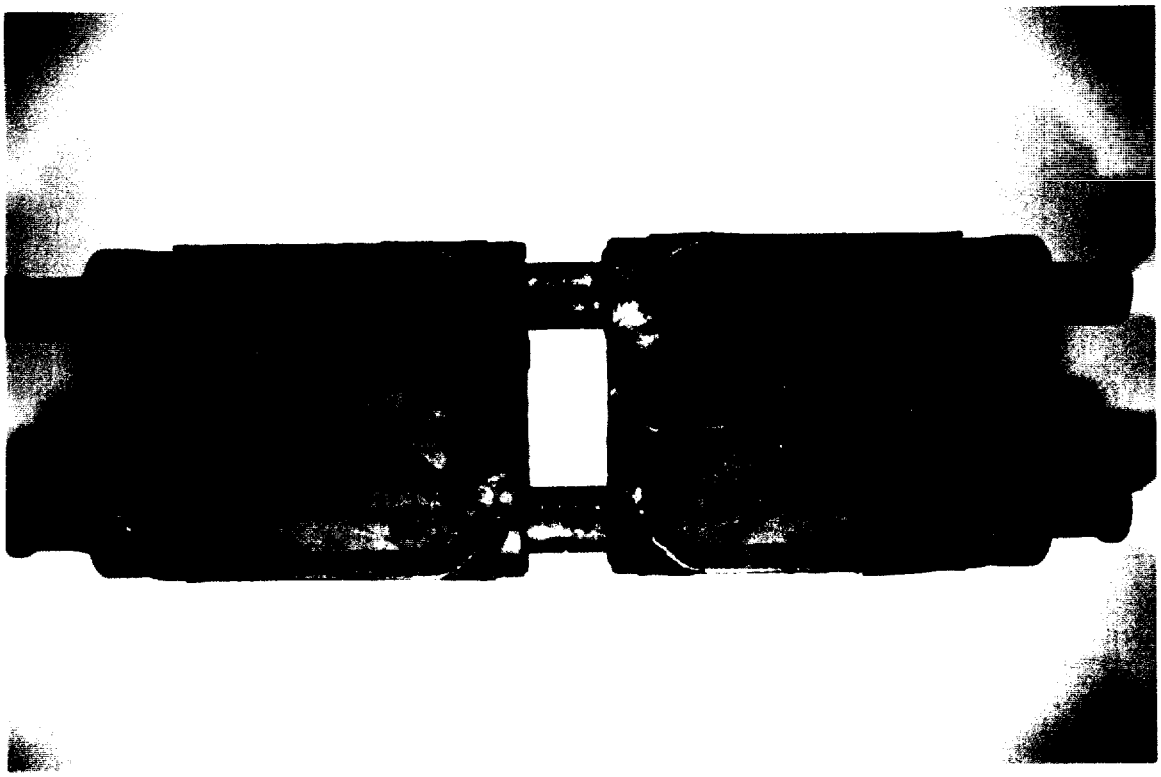

FIGURE 2 Failed track shoe #R6 in the as-received condition. Reduced 80%

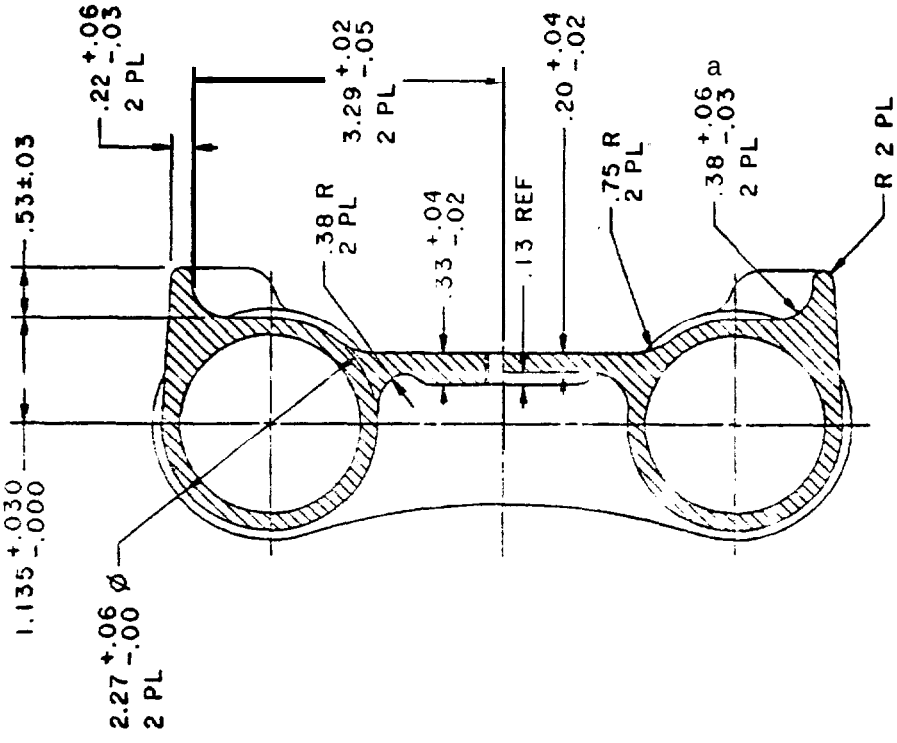

FIGURE 3 Schematic showing dimensions of the CAD1 track shoes.

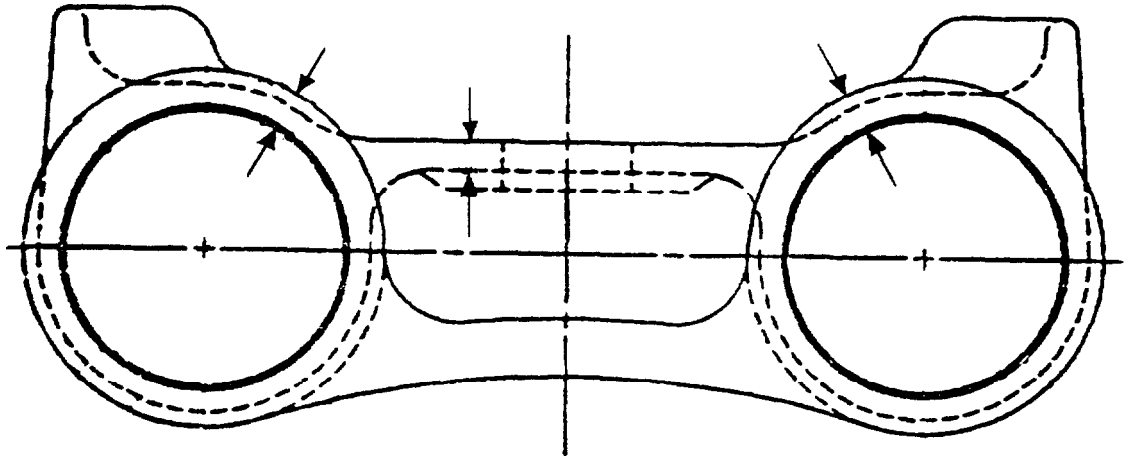

FIGURE 4 Schematic showing regions of dimensional inspection for each of the failed track shoes.

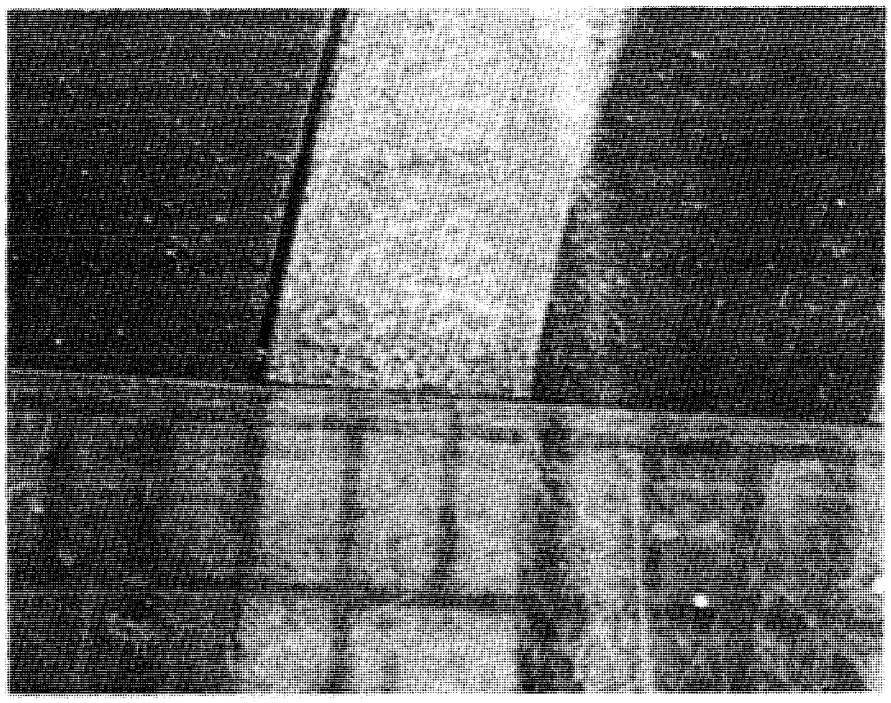

FIGURE 5 Macrograph showing area of minimum thickness on the binocular tube of track shoe #R6. Mag. 10x. (Scale in millimeters).

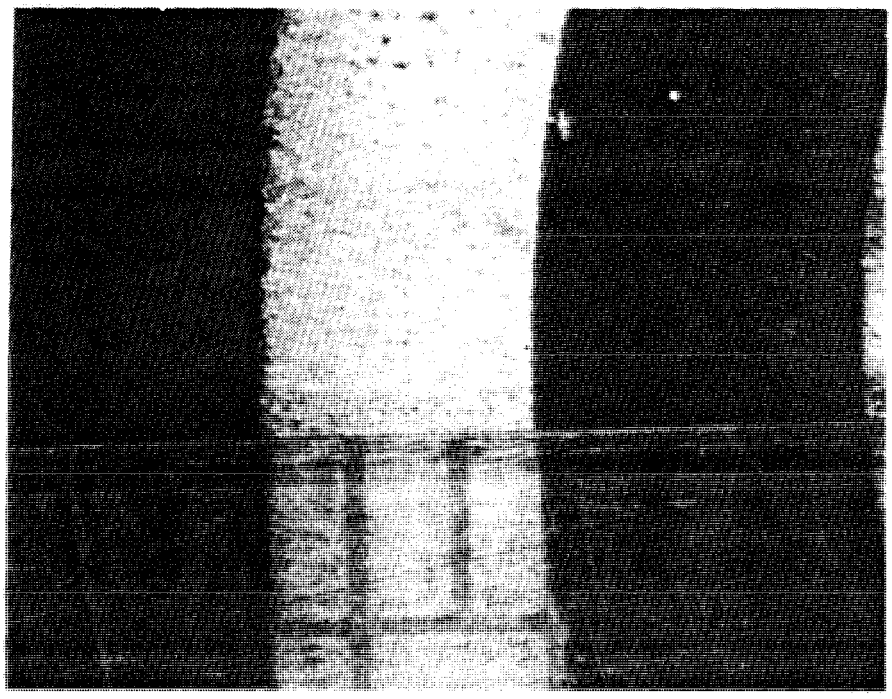

FIGURE 6 Macrograph showing thickness of the #R6 binocular tube on the ground side. Mag. 10x. (Scale in millimeters).

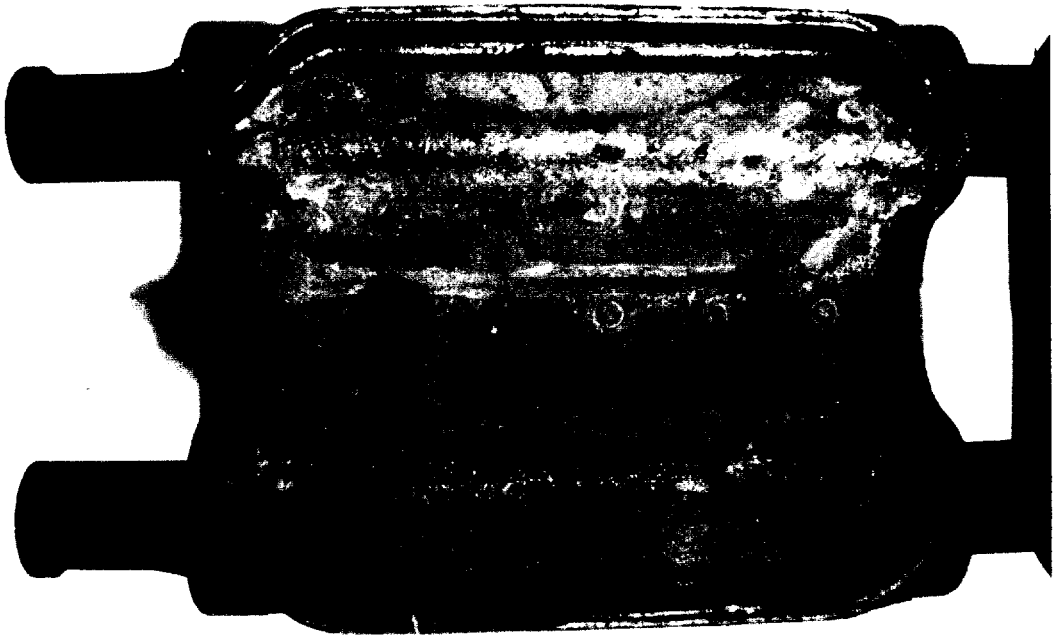

FIGURE 7 Macrograph showing failed half of track shoe #L30. Reduced 60%

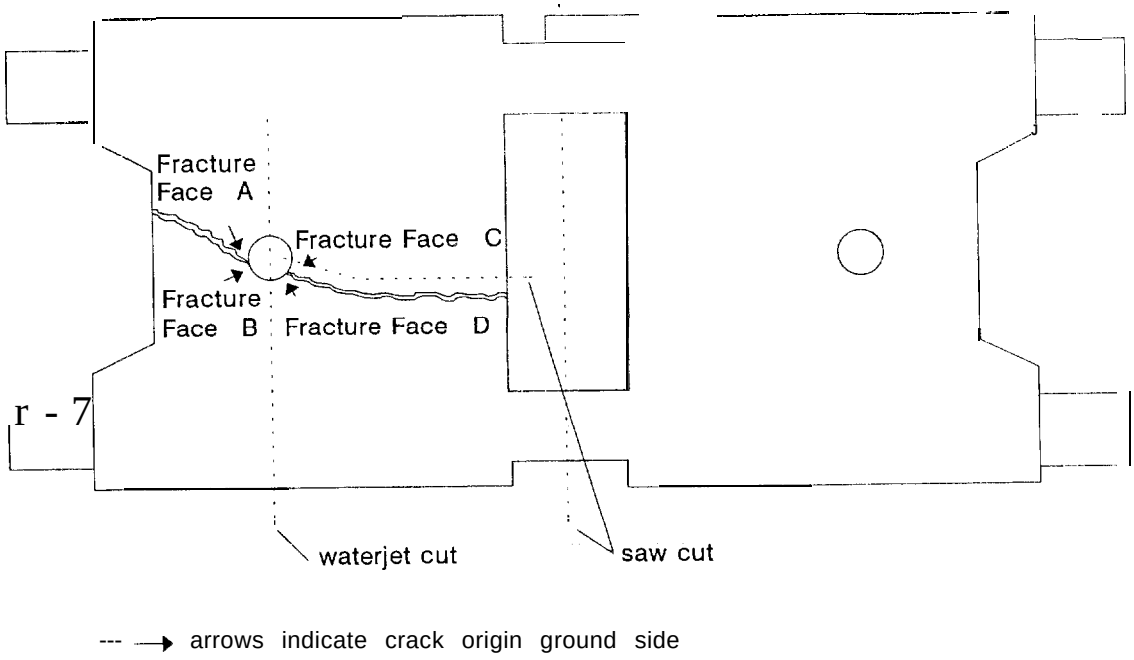

FIGURE 8 Schematic showing method used to section the fracture surfaces apart from track shoe #L30.

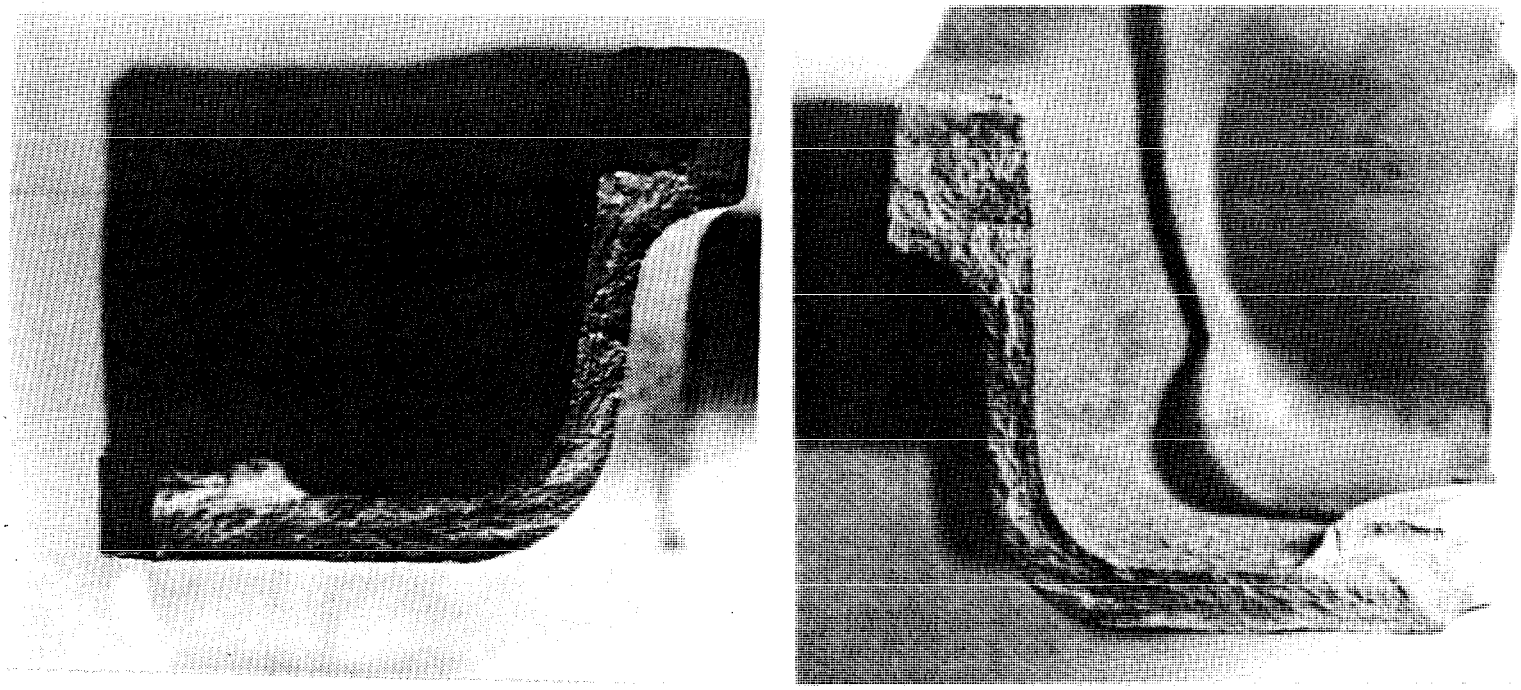

Fracture Face A Fracture Face B

FIGURE 9 Fracture faces A and B, respectively, of track shoe #L30. Chevron pattern converges to ground side of track shoe bolt hole. Mag. 1.25x.

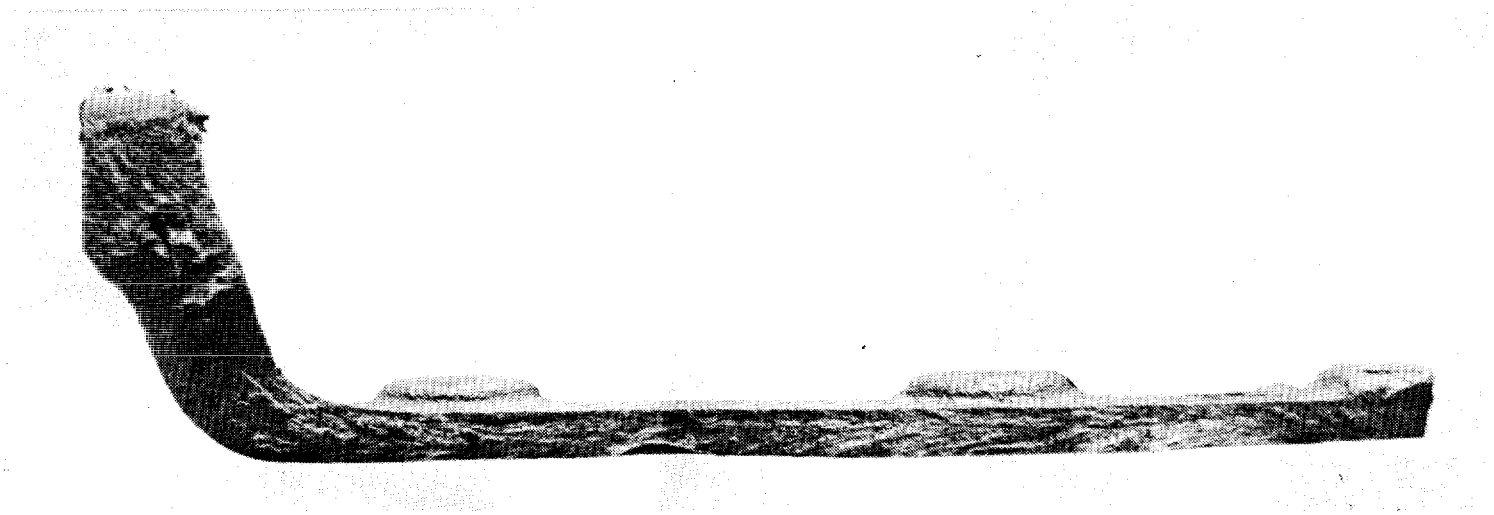

FIGURE 10 Macrograph of Fracture Face C of track shoe #L30. Chevron pattern converges to ground side of track shoe bolt hole. Mag. 1.25x.

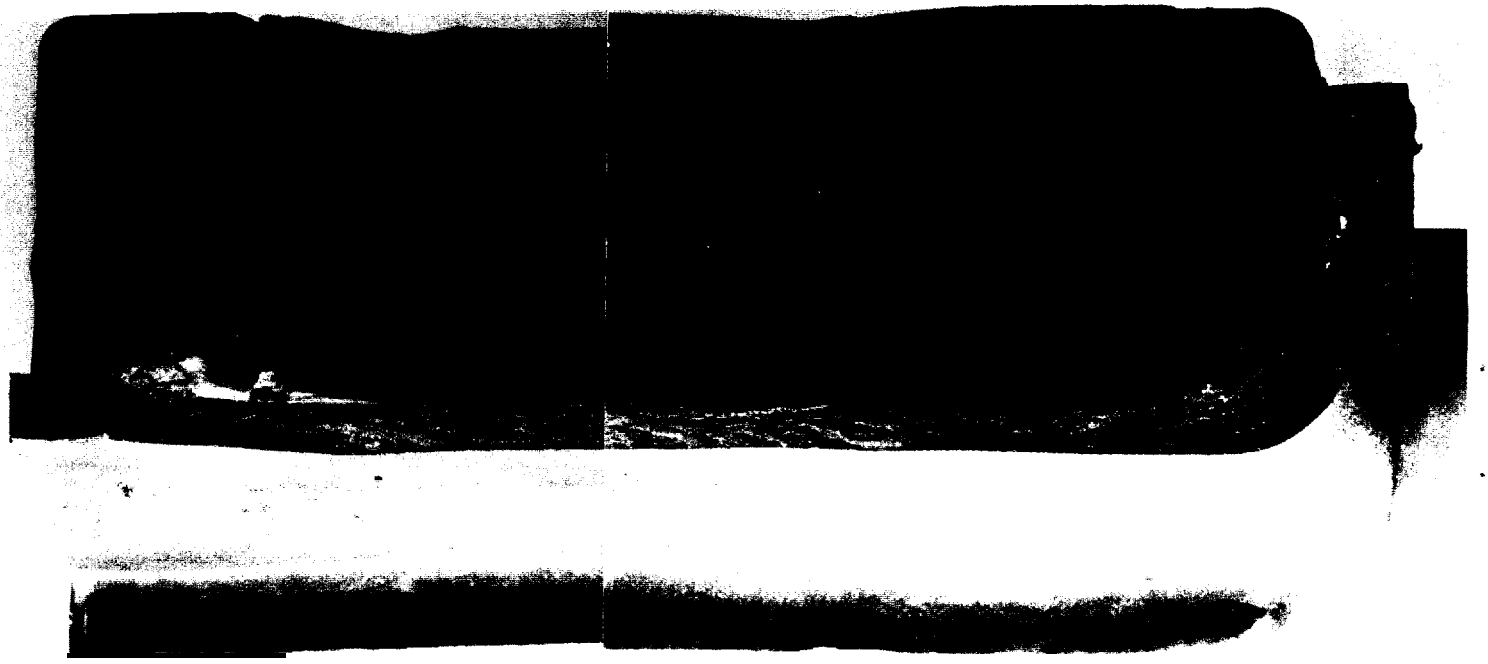

FIGURE 11 Fracture Face D of track shoe #L30. Chevron pattern converges to ground side of track shoe bolt hole. Mag. 1.25x.

FIGURE 12 Magnified view of the crack extending from the bolt hole of track shoe #L30 (ground side). Mag. lx.

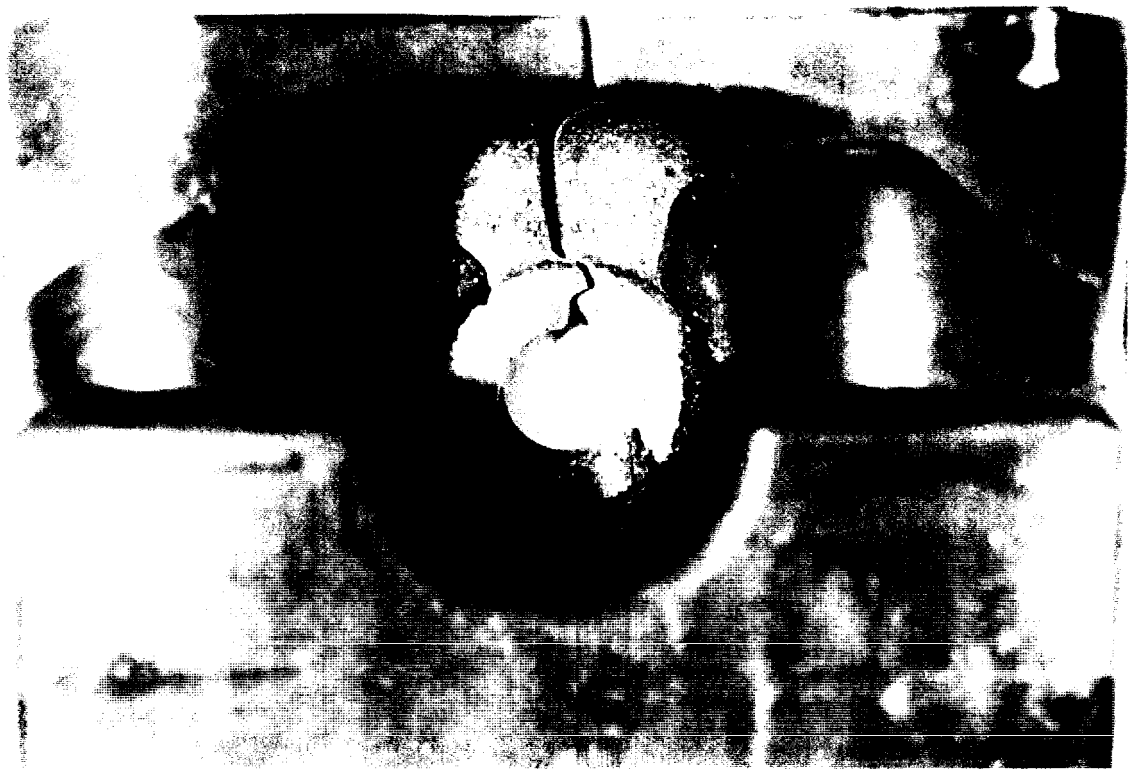

FIGURE 13 Magnified view of the underside of the cracked bolt hole of track shoe #L30 (wheel side). Mag. lx.

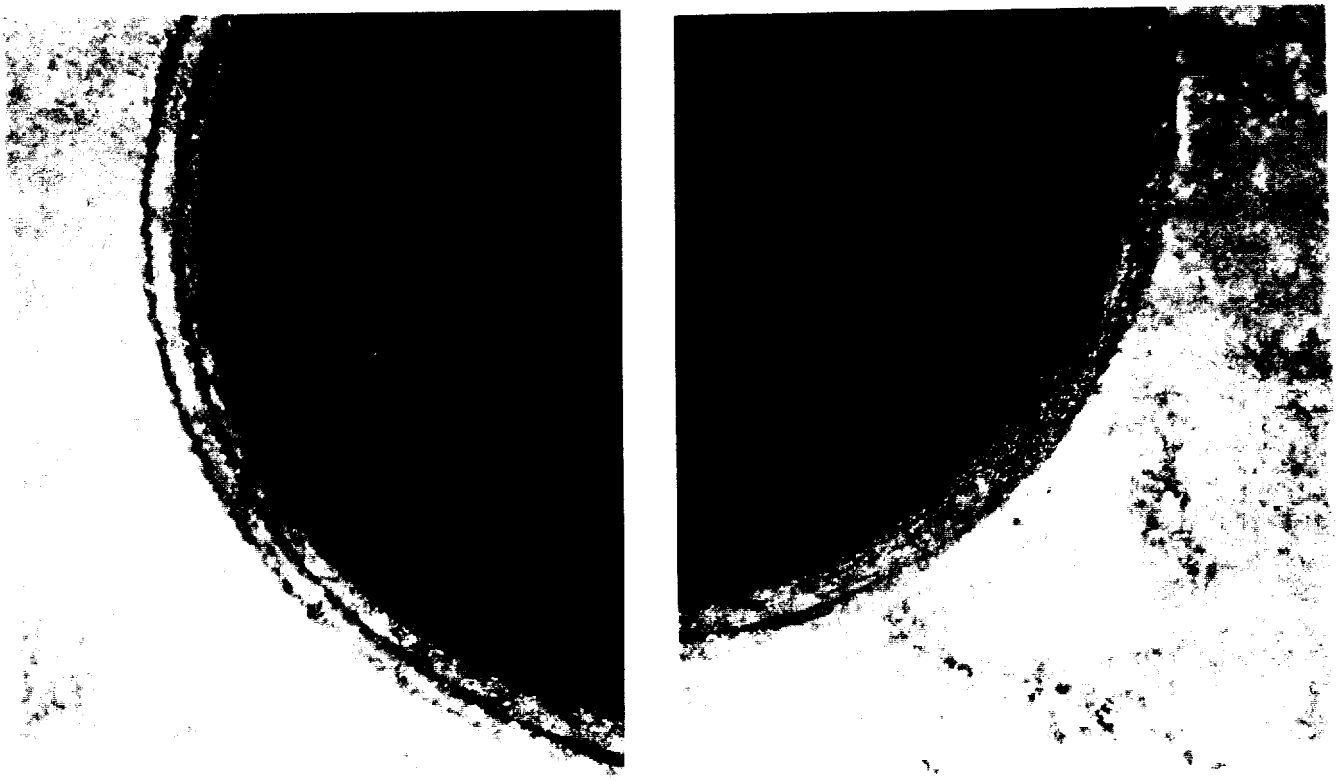

Track Shoe #L30 Track Shoe #R6

FIGURE 14 Comparison of the bolt holes of each track shoe. Mag. 7.5x.

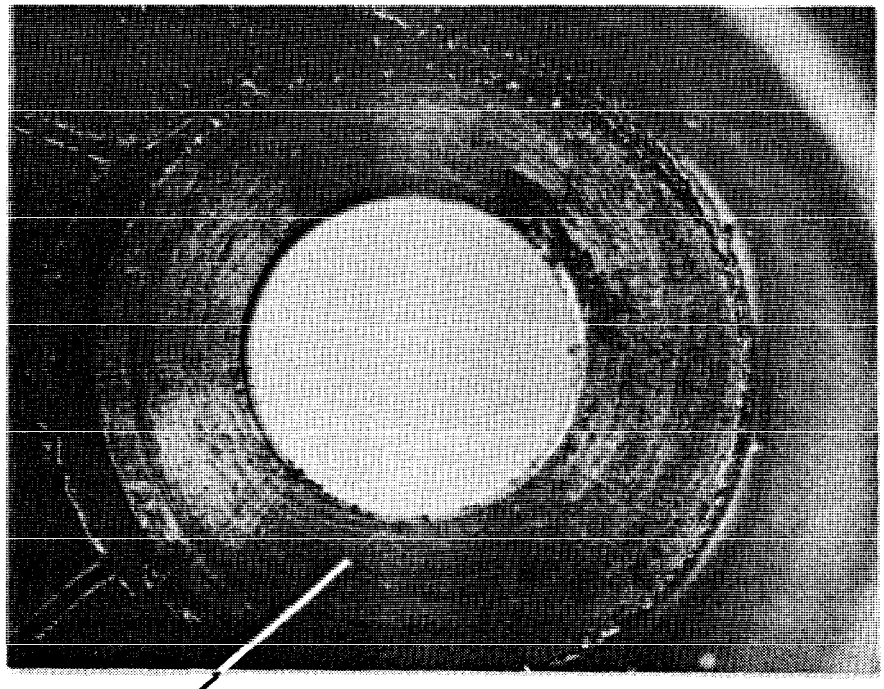

FIGURE 15 Blacklight photograph showing wear on underside of bolt hole. Notice the secondary crack revealed through magnetic particle inspection. Mag. 2x.

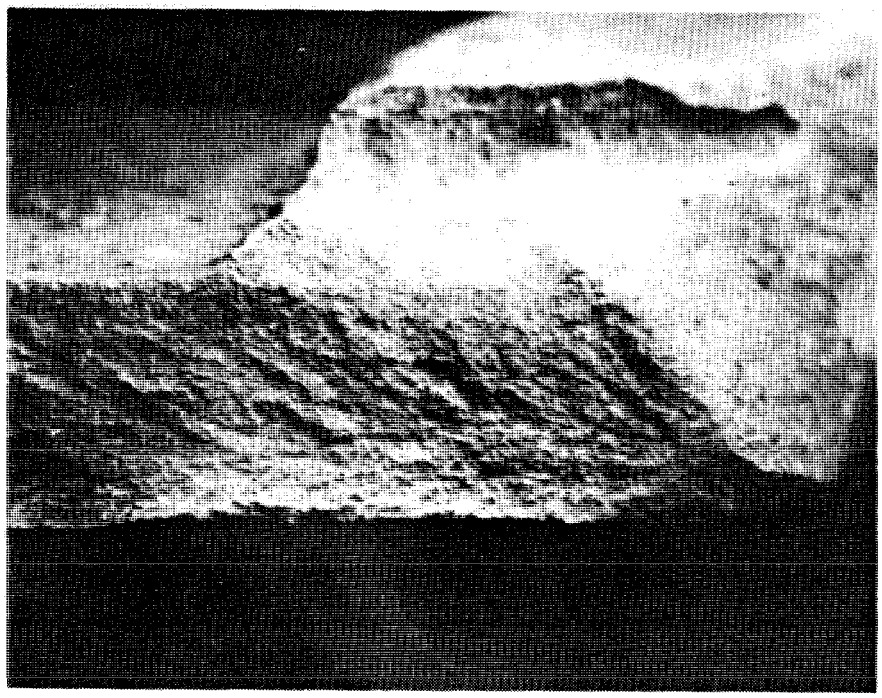

FIGURE 16 Enlargement of the crack origin on Fracture Face B. Mag. 10x.

FIGURE 17 Macrograph of fracture origin on Fracture Face D. Mag . 10x.

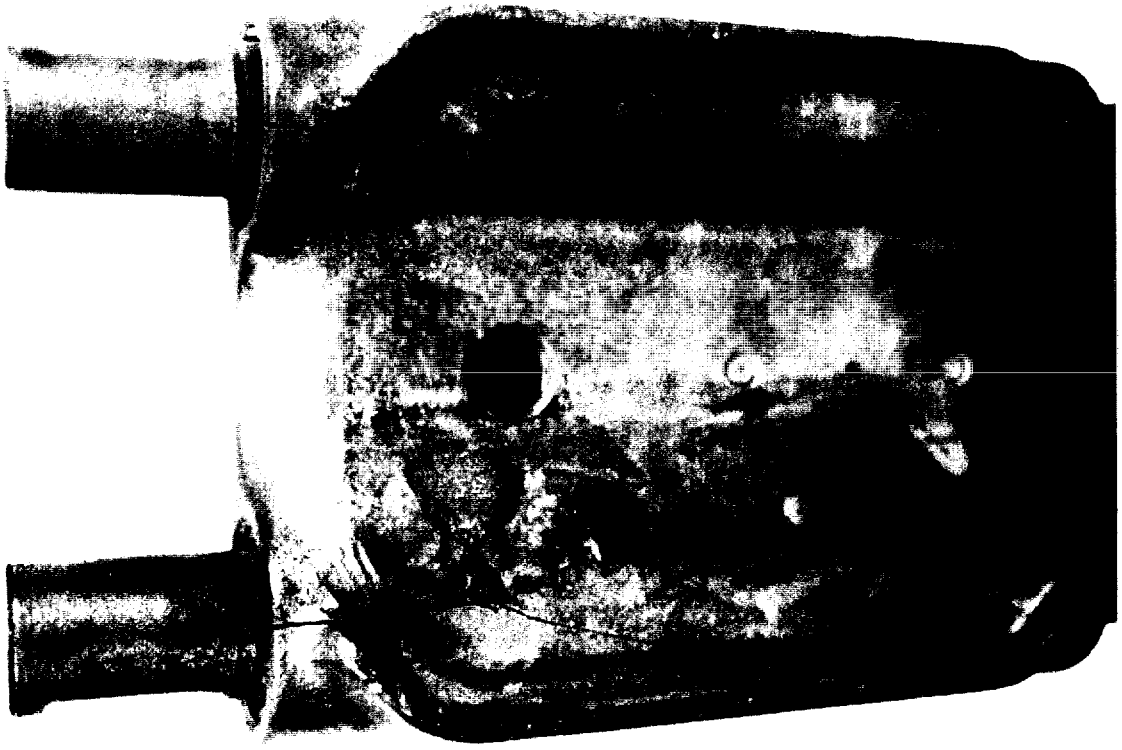

FIGURE 18 Macrograph showing failed half of track shoe #R6. Reduced 60%.

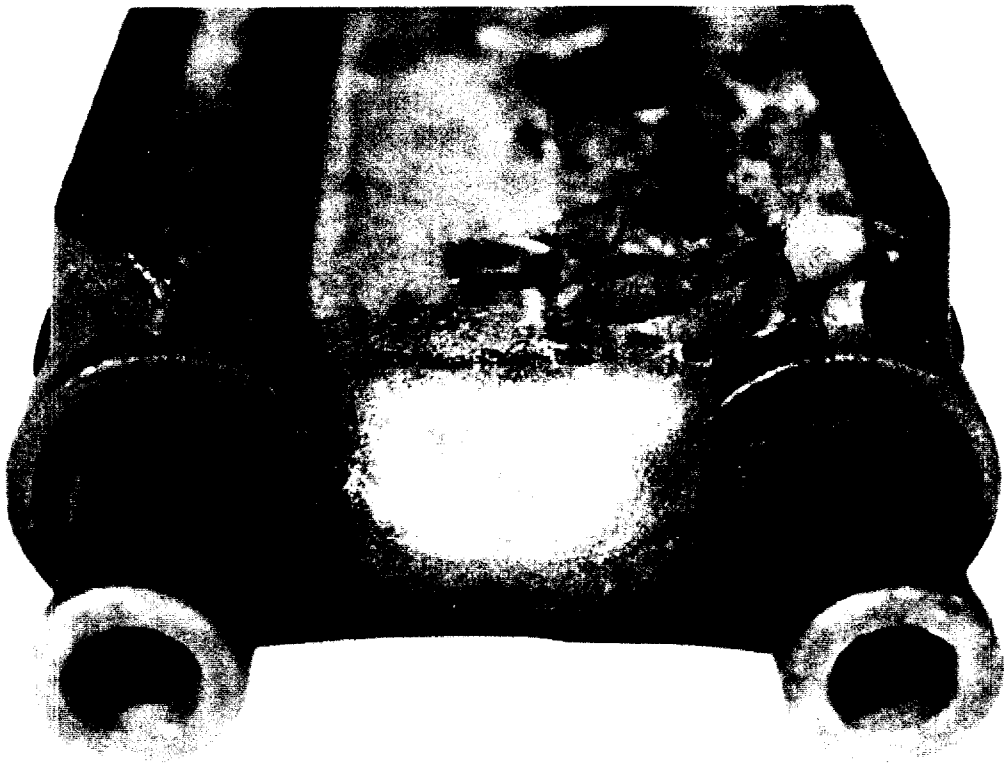

FIGURE 19 End view of track shoe #R6 showing cracking. Reduced 60%

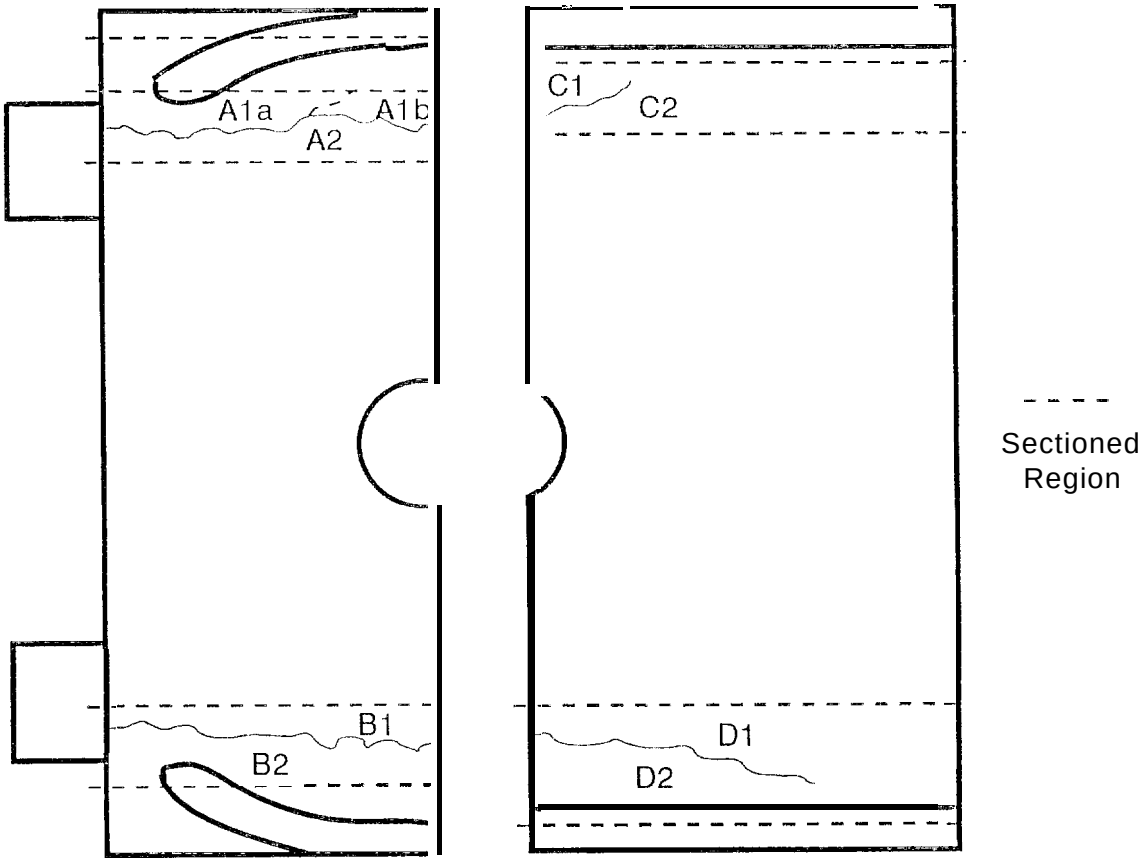

FIGURE 20 Schematic showing method of sectioning for the fracture surfaces of track shoe #R6.

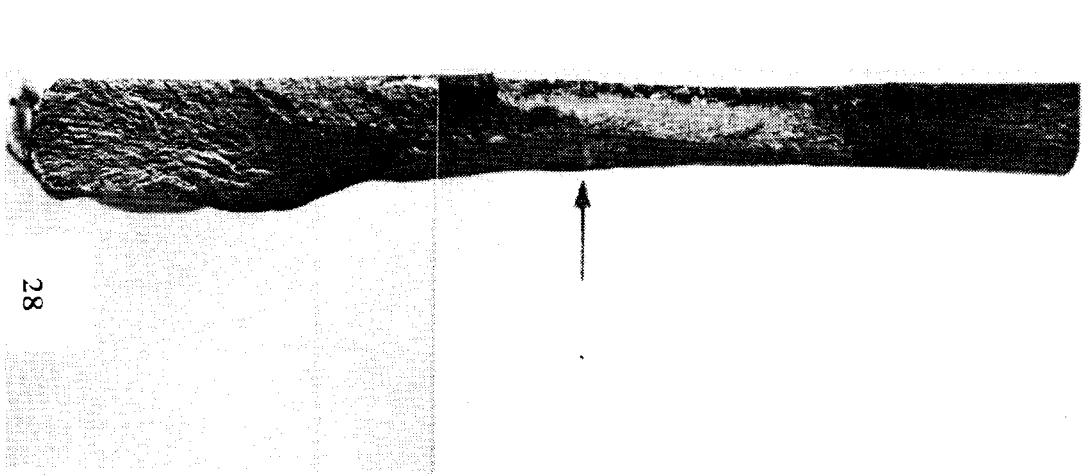

Figure 2 Photo montage showing fracture faces A and C. Arrow indicates fracture origin, as highlighted by chevron patterns and river markings. Mag. 2x.

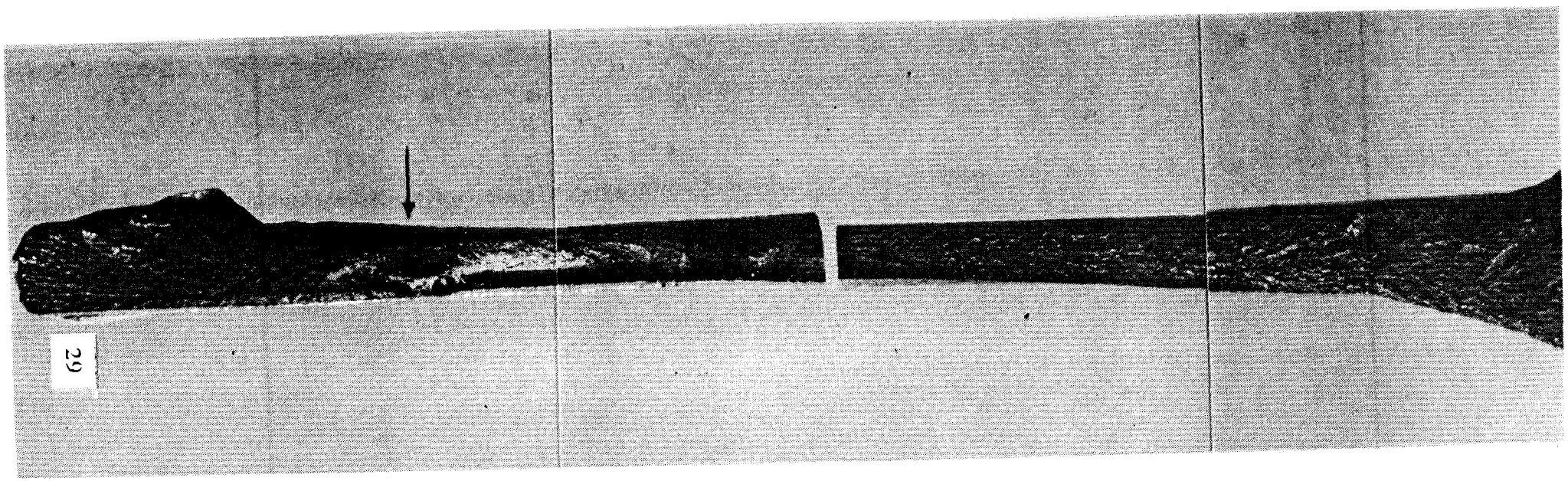

Figure 22 Photo montage showing fracture faces B and D. Arrow indicates fracture origin, as highlighted by chevron patterns and river markings. Mag. 2x.

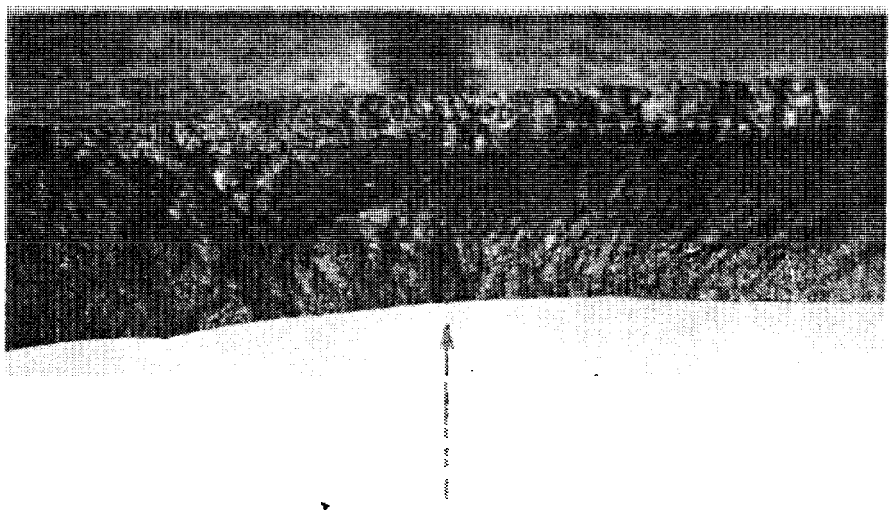

FIGURE 23 Fracture origin of fracture face A, of track shoe #R6. Mag. 7.5x.

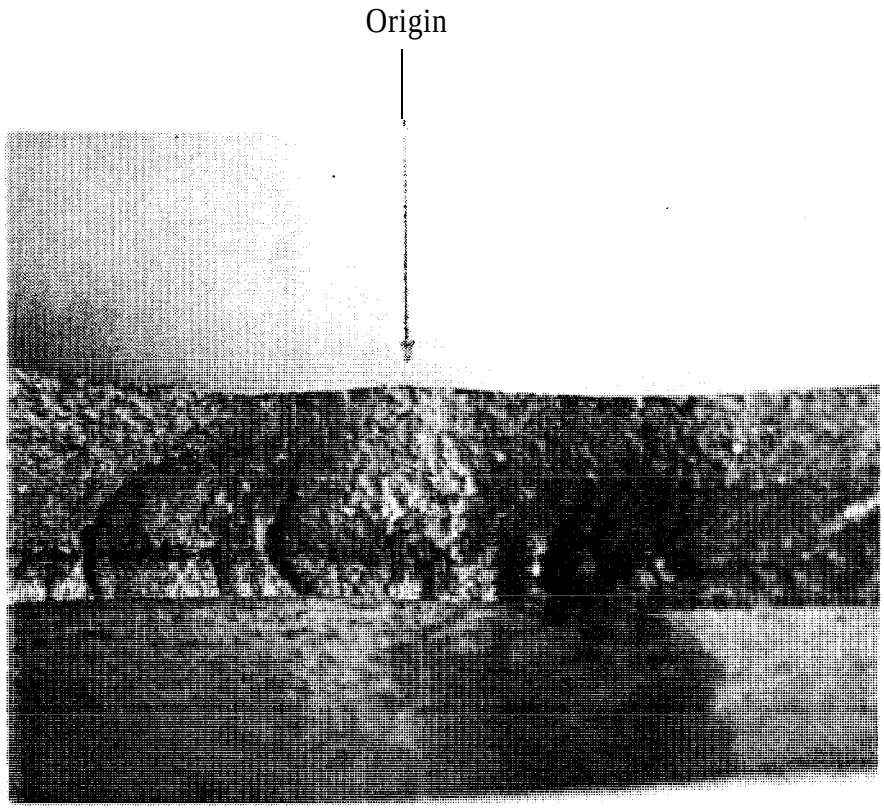

FIGURE 24 Fracture origin of fracture face B, of track shoe #R6. Mag. 7.5x

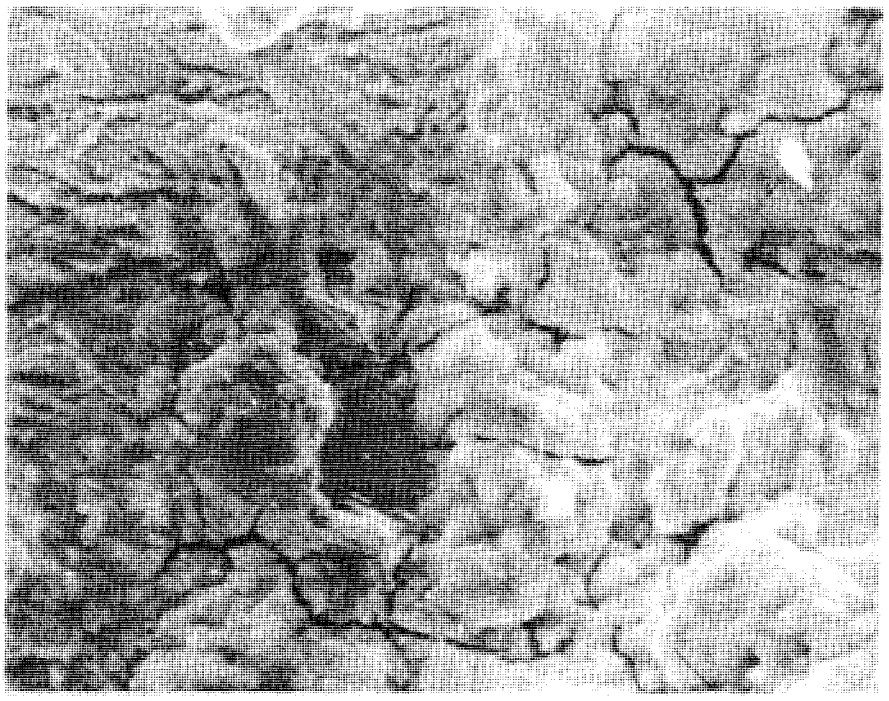

FIGURE 25 SEM of corroded fracture surface showing prevalent “mud-cracking”. Mag. 2500x.

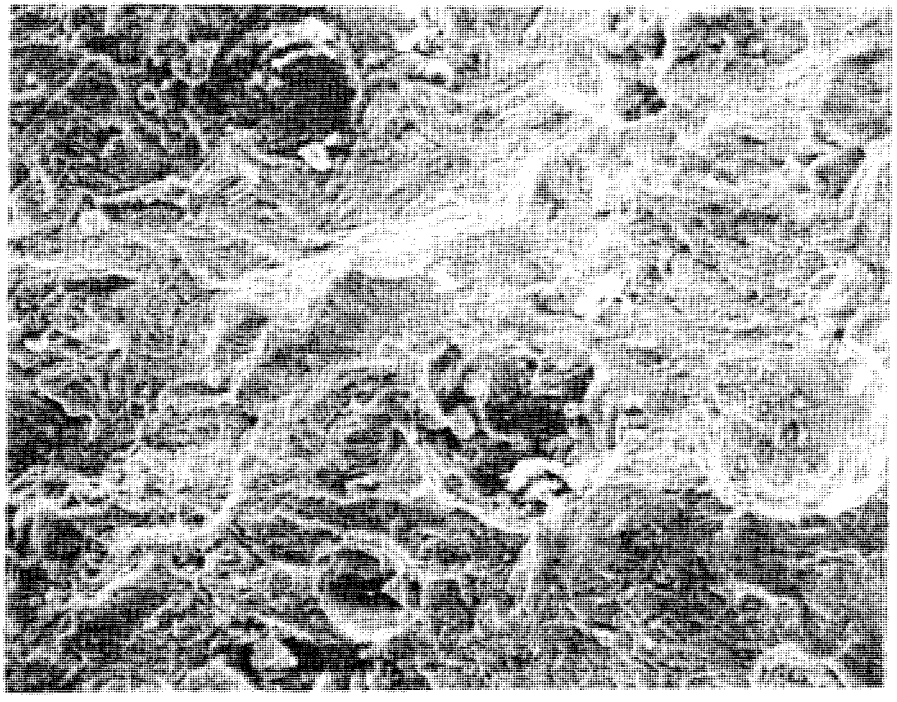

FIGURE 26 SEM showing representative morphology of a less corroded region of the fracture surfaces. Mag . 500x.

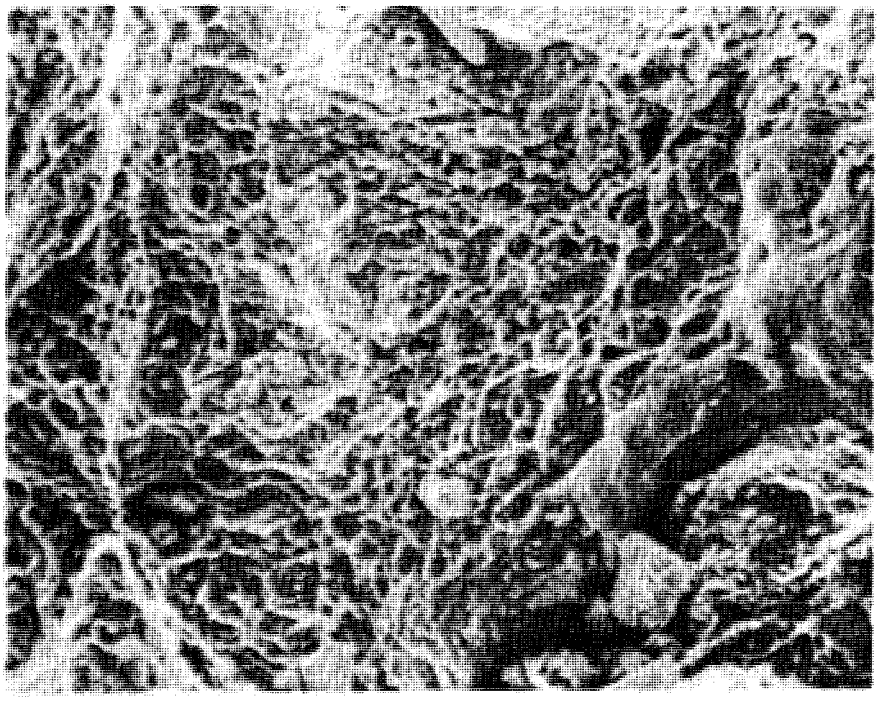

FIGURE 27 SEM showing area of ductile dimples suggesting overload failure. Mag. 2000x.

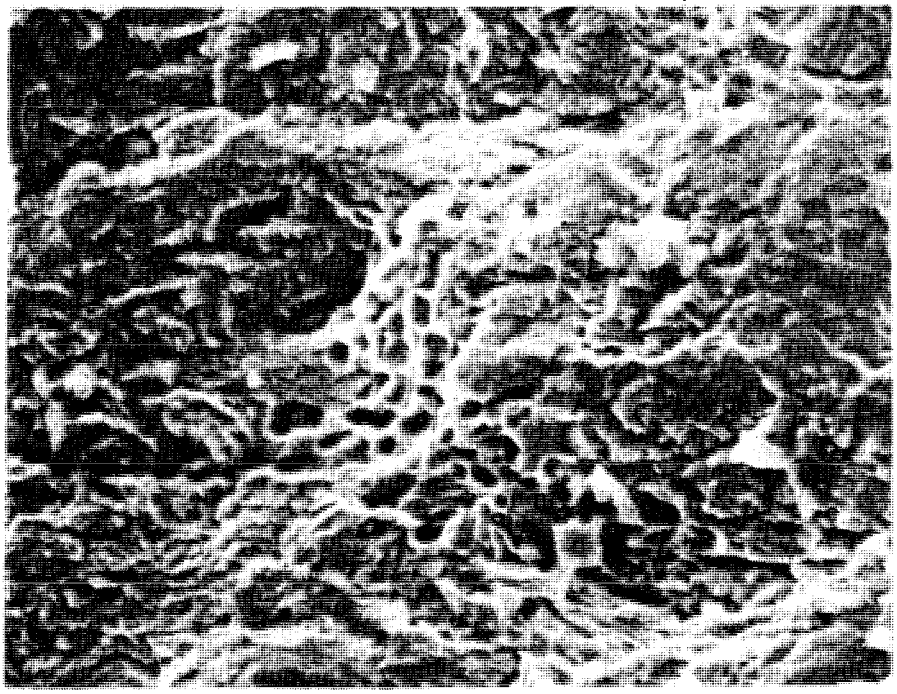

FIGURE 28 SEM of another area of ductile dimples noted on a less corroded region of the fracture surfaces. Mag. 2000x.

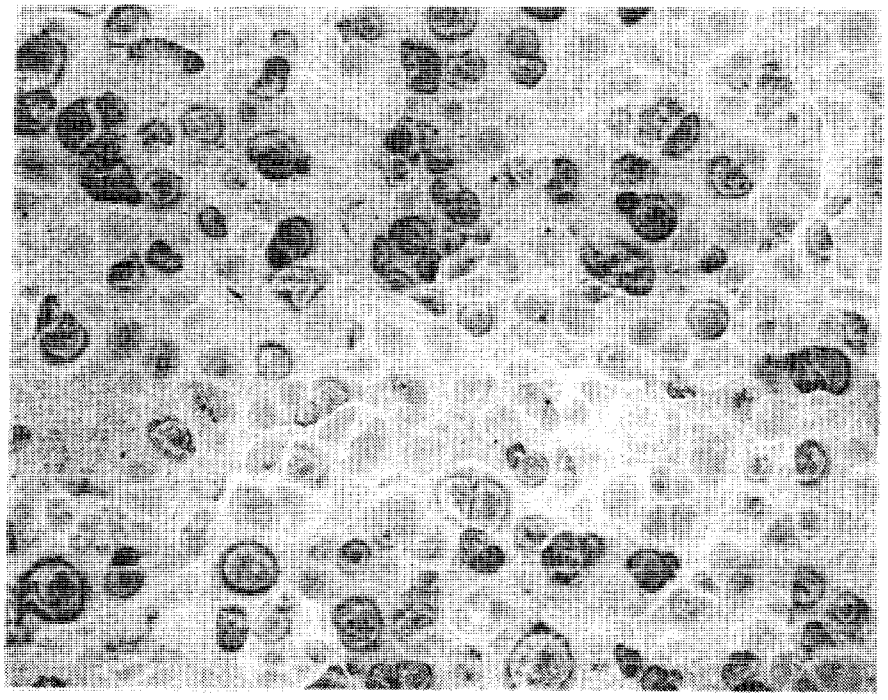

FIGURE 29 Low magnification SEM photograph of the fracture surface of a laboratory tested impact specimen. Mag. 150x.

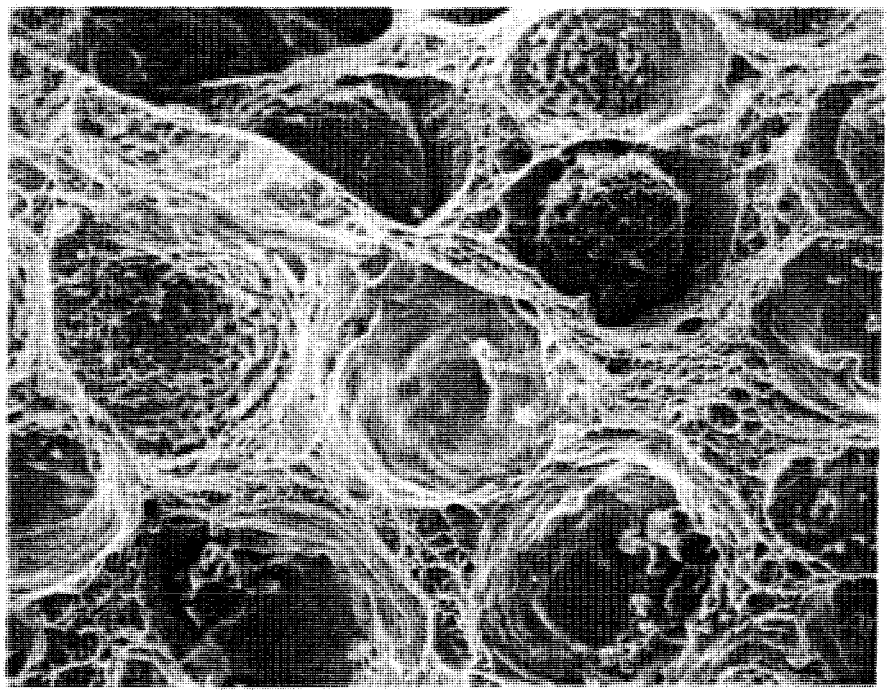

FIGURE 30 High magnification SEM photograph of the fracture surface of a laboratory tested impact specimen. Note the ductile dimples, similar to those found on the fracture surface of the failed track shoes. Mag. 800x.

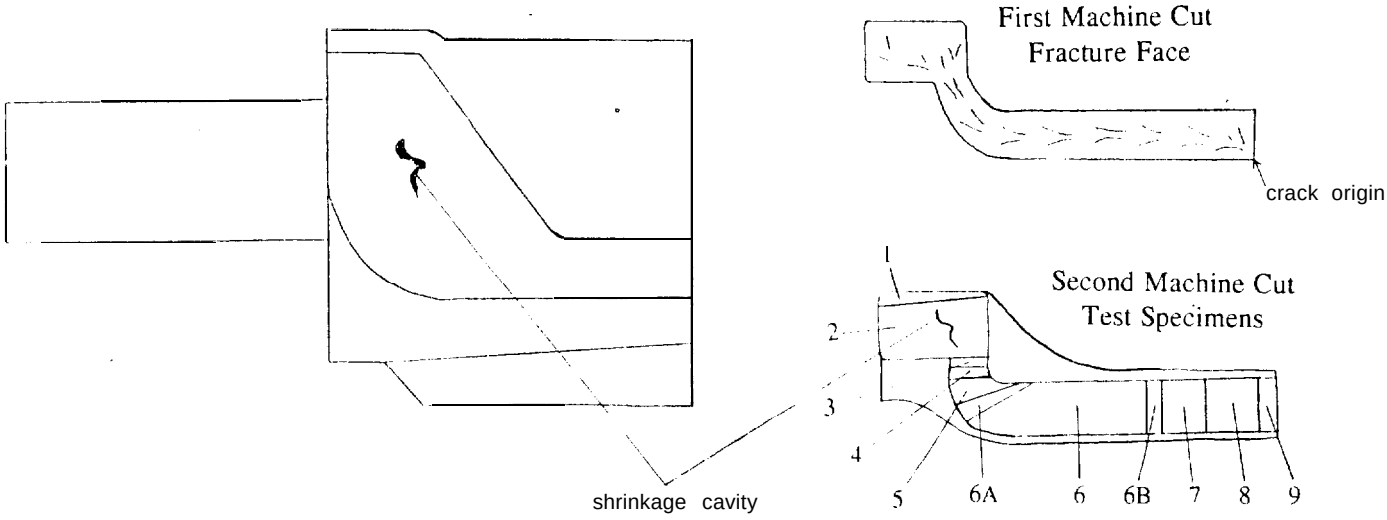

FIGURE 3 1 Schematic of sectioning diagram for metallographic and retained austenite samples from track shoe #L30. Similar specimens were sectioned from track shoe #R6.

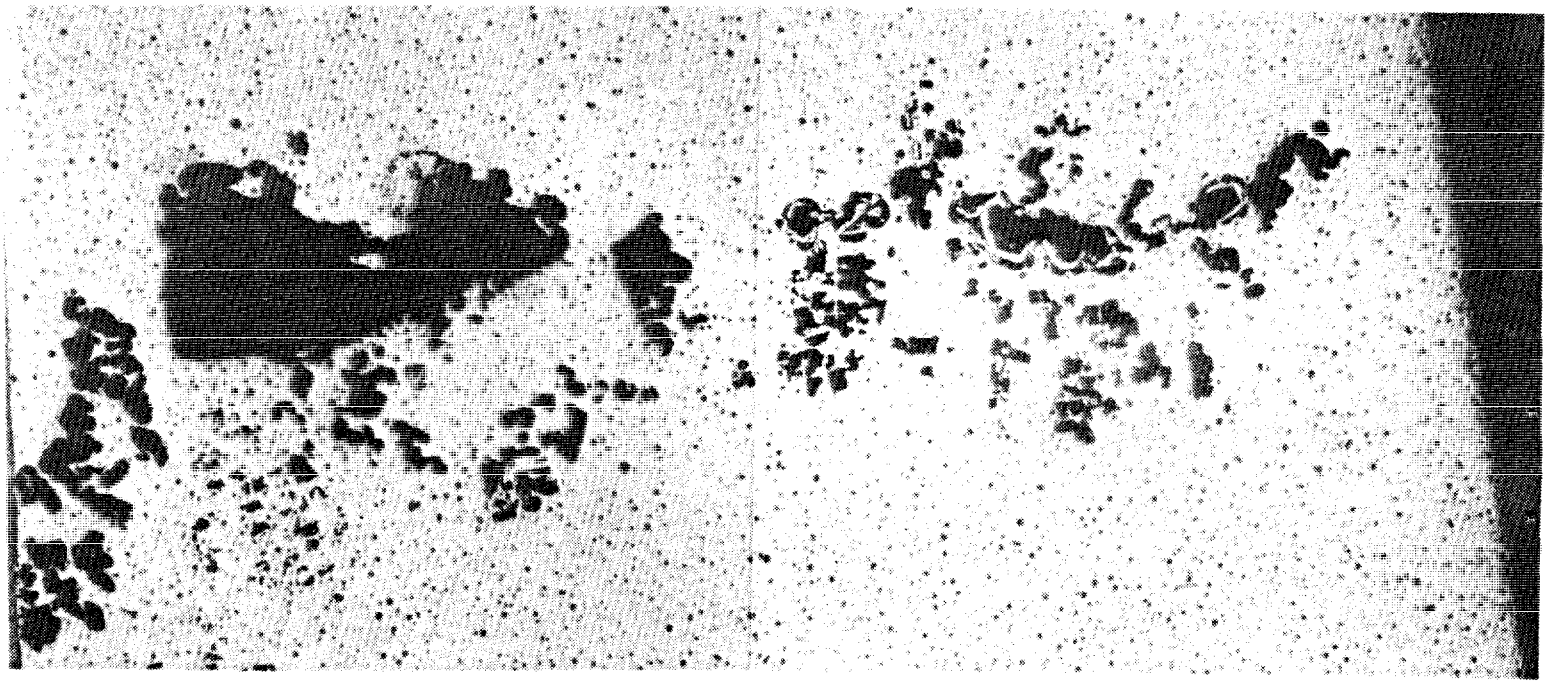

FIGURE 32 Large shrinkage cavity noted on track shoe #L30 metallographic specimen. Mag. 12.5x.

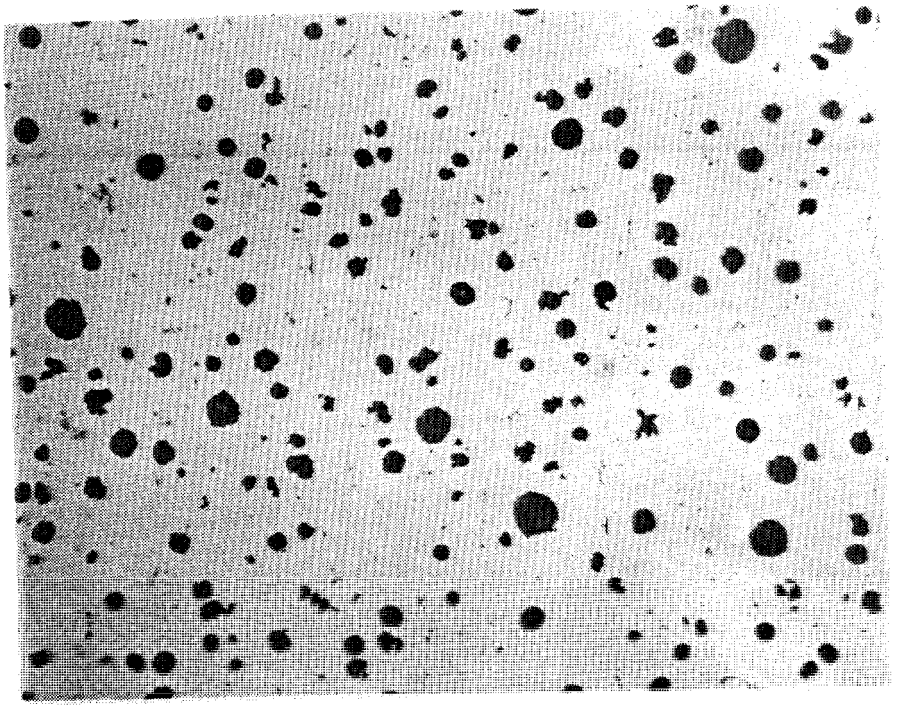

FIGURE 33 As-polished representative microstructure of a CAD1 sample, showing the graphite nodules. Nodule count was determined to be 132 per sq. mm., while nodule size was approximately 5 to 6, according to ASTM A 247. Mag. 100x.

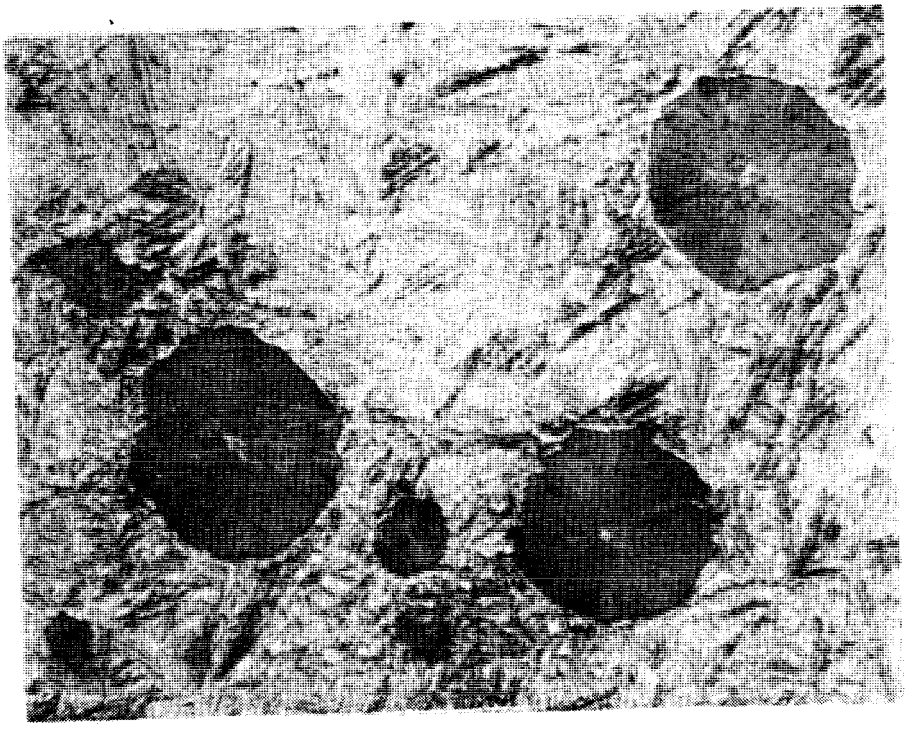

FIGURE 34 Typical microstructure of track shoe CADI with the application of a 4% Picral ‘etchant. Mag. 500x.

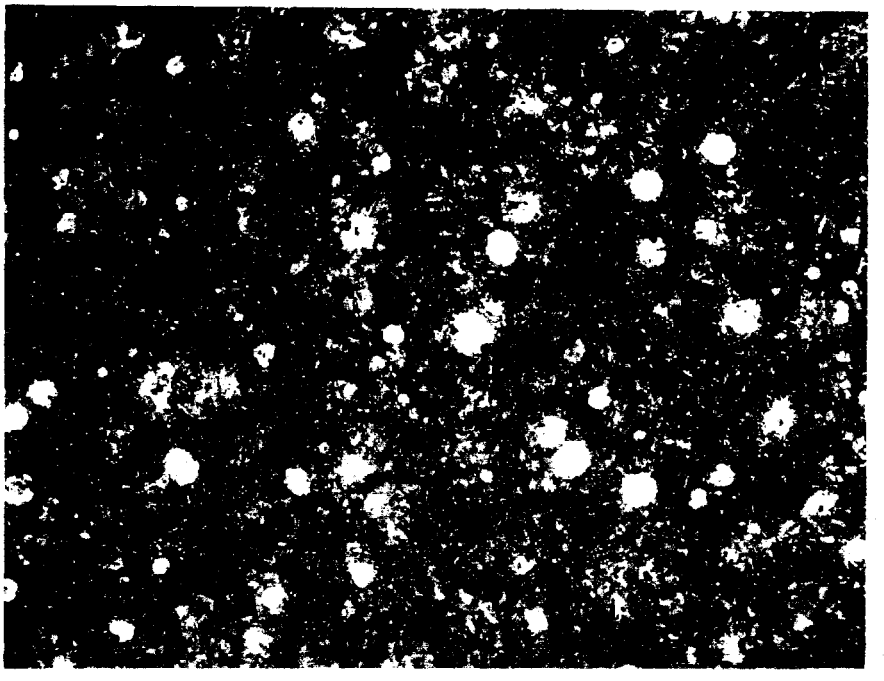

FIGURE 35 Typical structure of CAD1 when polished, etched with 4% Picral and heat tinted at 500°F for 4 hours. Mag. 100x.

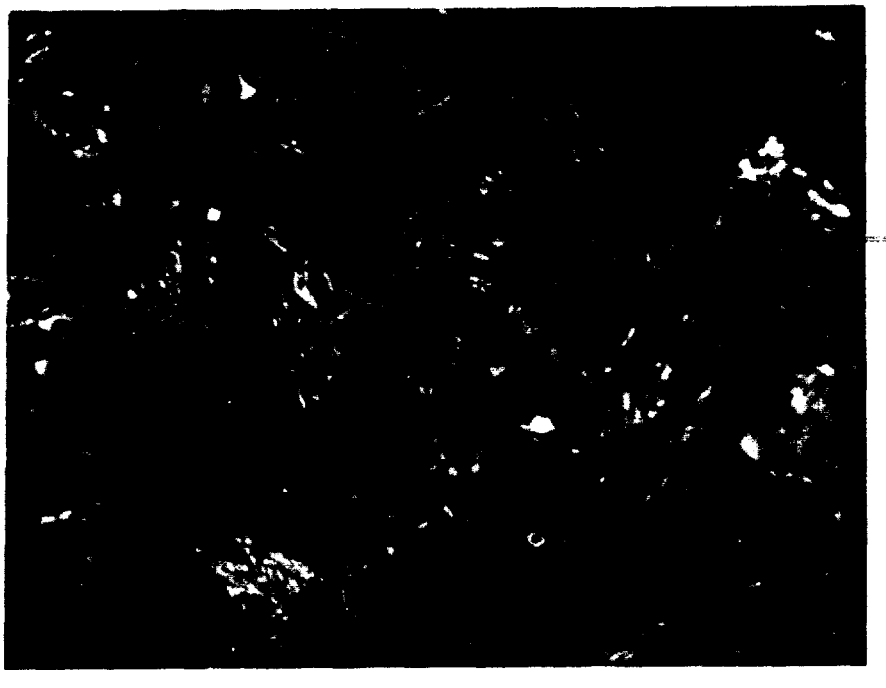

FIGURE 36 Higher magnification of structure of CADI when polished, etched with 4% Picral and heat tinted at 500°F for 4 hours. Mag. 1000x.

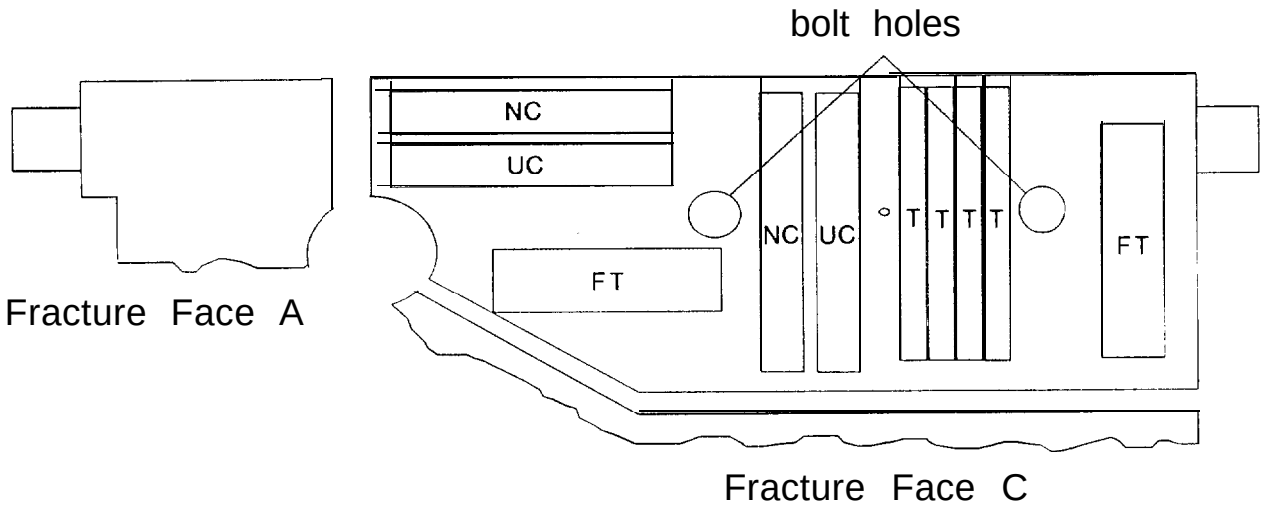

T = Tensile FT = Fracture Toughness
NC = Notched Charpy Impact
UN = Unnotched Charpy Impact

FIGURE 37 Mechanical property specimens sectioning diagram for track shoe #L30.

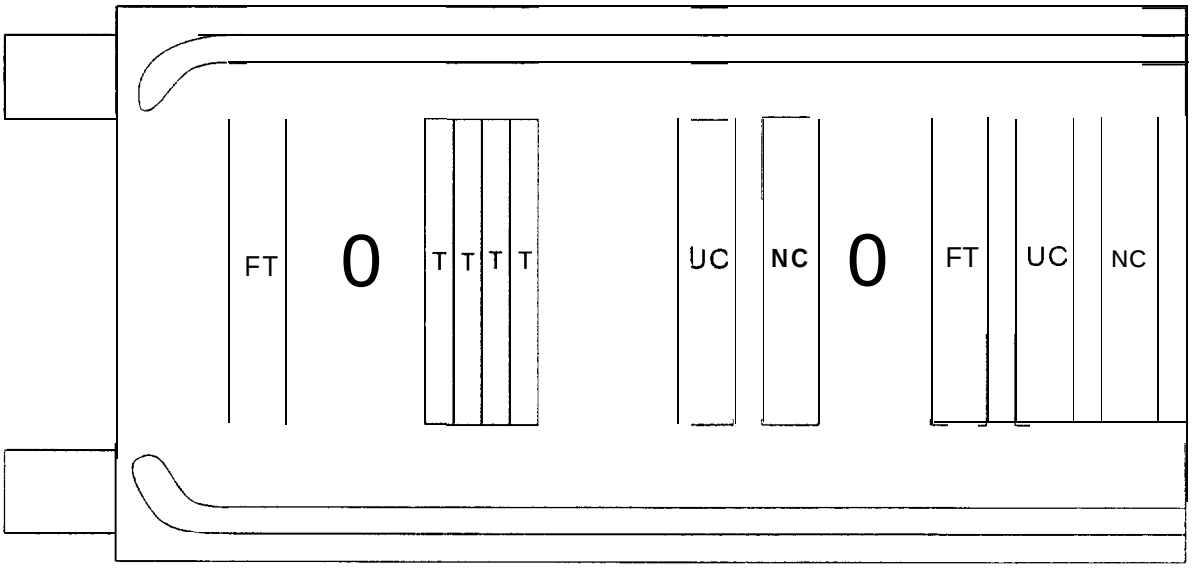

T=Tensile FT = Fracture Toughness
NC = Notched Charpy Impact
UN=Unnotched Charpy Impact

FIGURE 38 Mechanical property specimens sectioning diagram for track shoe #R6.

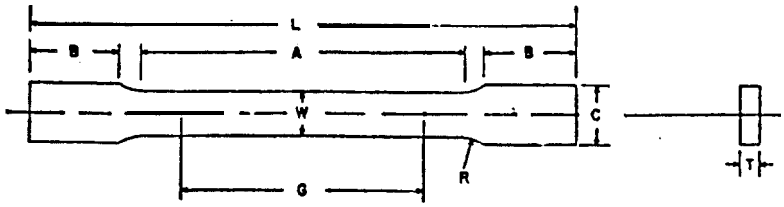

G=0.5"	L=2"
W =O. 125"	A =5/8"
T= 1/8"	B=5/8"
R= 1/8"	C=3/16"

FIGURE 39 Schematic of the tensile specimen utilized for CAD1 testing.

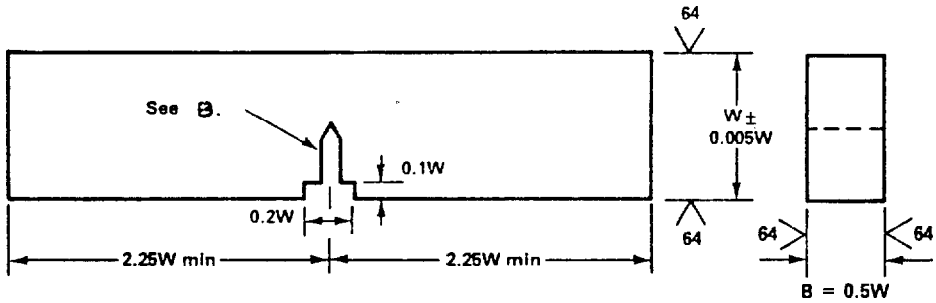

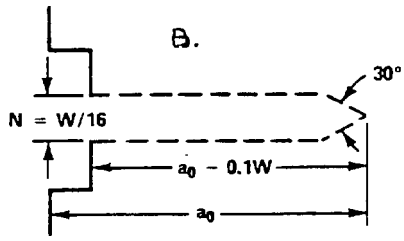

Notch

B=0.2"	0.1W=0.04"
w =0.4"	0.5W=0.2"
4.5W=1.8"	a_o=0.24
0.2W=0.08"	N=0.025
	a_o-0.1W=0.20

FIGURE 40 Schematic of the fracture toughness specimen utilized for CAD1 testing.

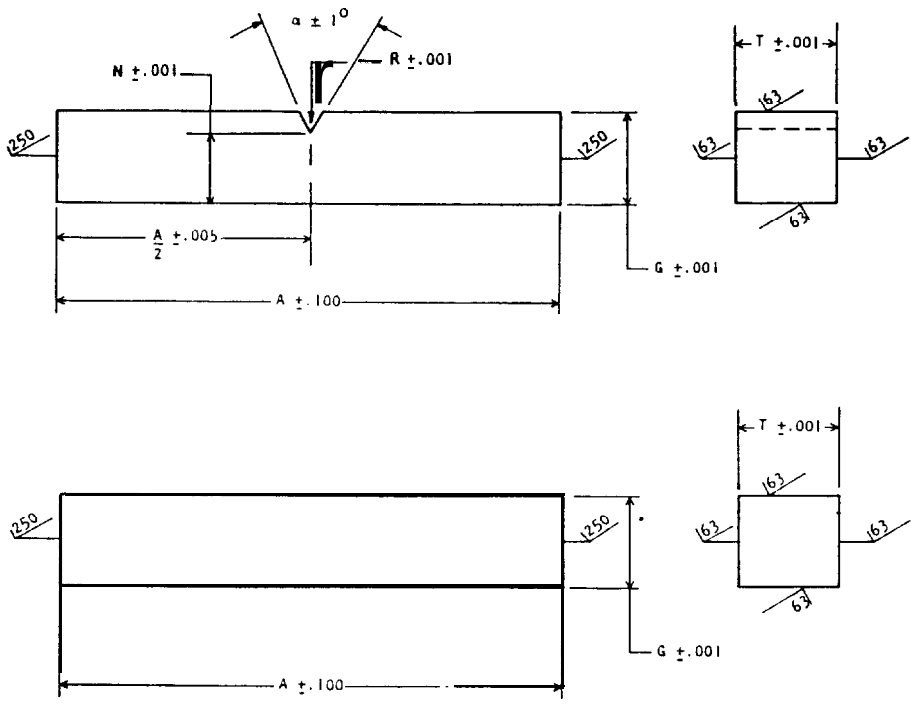

A=2.165" R=0.010"
G=0.394" T =O. 197”
N=0.315" ∝=45◦

FIGURE 41 Schematic of the notched and unnotched Charpy impact specimens used for CADI testing.

.DISTRIBUTION LIST

No. of Copies	To
1	Office of the Under Secretary of Defense for Research and Engineering, The Pentagon, Washington, DC 20301
	Director, U.S. Army Research Laboratory, 2800 Powder Mill Road, Adelphi, MD 20783-1197
1	ATTN: AMSRL-OP-SD-TP, Technical Publishing Branch
1	AMSRL-OP-SD-TM, Records Management Administrator
	Commander, Defense Technical Information Center, Cameron Station, Building 5, 5010 Duke Street, Alexandria, VA 23304-6145
2	ATTN: DTIC-FDAC
1	MIA/CINDAS, Purdue University, 2595 Yeager Road, West Lafayette, IN 47905
	Commander, Army Research Office, P.O. Box 12211, Research Triangle Park, NC 27709-2211
1	ATTN: Information Processing Office
	Commander, U.S. Army Materiel Command, 5001 Eisenhower Avenue, Alexandria, VA 22333
1	ATTN: AMCSCI
	Commander, U.S. Army Materiel Systems Analysis Activity, Aberdeen Proving Ground, MD 21005
1	ATTN: AMXSY-MP, H. Cohen
	Commander, U.S. Army Missile Command, Redstone Arsenal, AL 35809
1	ATTN: AMSMI-RD-CS-R/Doc
	Commander, U.S. Army Armament, Munitions and Chemical Command, Dover, NJ 07801
2	ATTN: Technical Library
	Commander, U.S. Army Natick Research, Development and Engineering Center, Natick, MA 01760-5010
1	ATTN: DFAS-IN-EM-TL, Technical Library
	Commander, U.S. Army Satellite Communications Agency, Fort Monmouth, NJ 07703
1	ATTN: Technical Document Center
	Commander, U.S. Army Tank-Automotive Command, Warren, MI 48397-5000
1	ATTN: AMSTA-ZSK
1	AMSTA-TSL, Technical Library
	President, Airborne, Electronics and Special Warfare Board, Fort Bragg, NC 28307
1	ATTN: Library
	Director, U.S. Army Research Laboratory, Weapons Technology, Aberdeen Proving Ground, MD 21005-5066
1	ATTN: AMSRL-WT

No. of Copies	To
	Commander, Dugway Proving Ground, UT 84022
1	ATTN: Technical Library, Technical Information Division
	Commander, U.S. Army Research Laboratory, 2800 Powder Mill Road, Adelphi, MD 20783
1	ATTN: AMSRL-SS
	Director, Benet Weapons Laboratory, LCWSL, USA AMCCOM, Watervliet, NY 12189
1	ATTN: AMSMC-LCB-TL
1	AMSMC-LCB-R
1	AMSMC-LCB-RM
1	AMSMC-LCB-RP
	Commander, U.S. Army Foreign Science and Technology Center, 220 7th Street, N.E., Charlottesville, VA 22901-5396
3	ATTN: AIFRTC, Applied Technologies Branch, Gerald Schlesinger
	Commander, U.S. Army Aeromedical Research Unit, P.O. Box 577, Fort Rucker, AL 36360
1	ATTN: Technical Library
	U.S Army Aviation Training Library, Fort Rucker, AL 36360
1	ATTN: Building 5906-5907
	Commander, U.S. Army Agency for Aviation Safety, Fort Rucker, AL 36362
1	ATTN: Technical Library
	Commander, Clarke Engineer School Library, 3202 Nebraska Ave., N, Fort Leonard Wood, MO 65473-5000
1	ATTN: Library
	Commander, U.S. Army Engineer Waterways Experiment Station, P.O. Box 631, Vicksburg, MS 39180
1	ATTN: Research Center Library
	Commandant, U.S. Army Quartermaster School, Fort Lee, VA 23801
1	ATTN: Quartermaster School Library
	Naval Research Laboratory, Washington, DC 20375
2	ATTN: Dr. G. R. Yoder - Code 6384
	Chief of Naval Research, Arlington, VA 22217
1	ATTN: Code 471
	Commander, U.S. Air Force Wright Research & Development Center, Wright-Patterson Air Force Base, OH 45433-6523
1	ATTN: WRDC/MLLP, M. Forney, Jr.
1	WRDC/MLBC, Mr. Stanley Schulman
	U.S. Department of Commerce, National Institute of Standards and Technology, Gaithersburg, MD 20899
1	ATTN: Stephen M. Hsu, Chief, Ceramics Division, Institute for Materials Science and Engineering

No. of Copies	To
1	Committee on Marine Structures, Marine Board, National Research Council, 2101 Constitution Avenue, N.W., Washington, DC 20418
1	Materials Sciences Corporation, Suite 250, 500 Office Center Drive, Fort Washington, PA 19034
1	Charles Stark Draper Laboratory, 555 Technology Square, Cambridge, MA 02139
	Wyman-Gordon Company, Worcester, MA 01601
1	ATTN: Technical Library
	General Dynamics, Convair Aerospace Division, P.O. Box 748, Fort Worth, TX 76101
1	ATTN: Mfg. Engineering Technical Library
	Plastics Technical Evaluation Center, PLASTEC, ARDEC, Bldg. 355N, Picatinny Arsenal, NJ 07806-5000
1	ATTN: Harry Pebly
1	Department of the Army, Aerostructures Directorate, MS-266, U.S. Army Aviation R&T Activity - AVSCOM, Langley Research Center, Hampton, VA 23665-5225
1	NASA - Langley Research Center, Hampton, VA 23665-5225
	U.S. Army Vehicle Propulsion Directorate, NASA Lewis Research Center, 2100 Brookpark Road, Cleveland, OH 44135-3191
1	ATTN: AMSRL-VP
	Director, Defense Intelligence Agency, Washington, DC 20340-6053
1	ATTN: ODT-5A (Mr. Frank Jaeger)
	U.S. Army Communications and Electronics Command, Fort Monmouth, NJ 07703
1	ATTN: Technical Library
	U.S. Army Research Laboratory, Electronic Power Sources Directorate, Fort Monmouth, NJ 07703
1	ATTN: Technical Library
	Director, U.S. Army Research Laboratory, Watertown, MA 02172-0001
2	ATTN: AMSRL-OP-WT-IS, Technical Library
30	Authors